# METASTABLE EUTECTIC EQUILIBRIUM IN NATURAL ENVIRONMENTS: RECENT DEVELOPMENTS AND RESEARCH OPPORTUNITIES

Joe. Your own copy

by

Frans J.M. Rietmeijer

Institute of Meteoritics, Department of Earth and Planetary Sciences,
University of New Mexico, Albuquerque, NM 87131, USA
Email: fransjmr@unm.edu

Joseph A. Nuth III

Astrochemistry Branch, Mail Stop 691,
NASA Goddard Space Flight Center, Greenbelt, MD 20771, USA
Email: u1jan@lepvax.gsfc.nasa.gov

Mariola Jablonska

Faculty of Earth Sciences, University of Silesia,
Bedzinska 60, 41-200 Sosnowiec, Poland
Email: mjablons@us.edu.pl

and

James M. Karner
Institute of Meteoritics, Department of Earth and Planetary Sciences,
University of New Mexico, Albuquerque, NM 87131, USA
Email: jkarner@unm.edu

Submitted to RESEARCH TRENDS; Trends in Geochemistry
January 15, 2000

Abstract Chemical ordering at metastable eutectics was recognized in non-equilibrium gas-to-solid condensation experiments to constrain 'silicate' dust formation in O-rich circumstellar environments. The predictable metastable eutectic behavior successfully predicted the observed ferromagnesiosilica compositions of circumstellar dust, presolar and solar nebula grains in the matrix of the collected aggregate IDPs. Many of the experimentally determined metastable eutectic solids match the fundamental building blocks of common rock-forming layer silicates: this could have implications for the origin of Life. The physical conditions conducive to metastable eutectic behavior, *i.e.* high temperature and (ultra)fast quenching, lead to unique amorphous, typically nano- to micrometer-sized, materials. The new paradigm of metastable eutectic behavior opens the door to new and exciting research opportunities in uncovering the many implications of these unique amorphous, and typically nano- to micrometer-sized, metastable eutectic materials.

## INTRODUCTION

Nature abhors a vacuum. Humans abhor unpredictable change. Equilibrium thermodynamics, which satisfies our desire for order, is a useful tool to describe the ideal state of a system wherein nothing changes. It does not, and can not, tell how a system was formed. The activation energy required going from one equilibrium-state to another one is ideally available instantaneously and systems would therefore adjust rapidly to changing environments. Metamorphic reactions are an extreme case wherein so-called *metamorphic overstepping* is necessary to provide the driving force to adjust the new mineralogy to the imposed conditions. These reactions will not occur at the pressure-temperature conditions predicted by experimentally determined phase stability curves. In order to reach a new thermodynamic equilibrium state the metamorphic reactions will most likely proceed via one or more intermediate stages of kinetically controlled reactions that by their non-equilibrium nature seem to be unpredictable. It might be tempting to give up any attempt to reconstruct the conditions and unpredictable chains of events of continual changes. But what happens when the new conditions are far removed from equilibrium?

This is not uncharted territory but a regime of a so-called *Prigogine dissipative structure*, which is a state of organization wherein disorder itself becomes a new source of order [1]. One obvious process characterized by severe non-equilibrium would be gas-to-solid condensation whereby variations in the rate of condensation or evaporation occur as a function of grain temperature below the thermal equilibrium temperature [2]. There will be a domain of grain growth wherein order will evolve via condensation when the rate of condensation exceeds the

evaporation rate [2]. These domains of order or *Prigogine dissipative structures* are represented as metastable solids. Prigogine dissipative structures may arise in many space environments [2] where dust is formed by vapor phase condensation. This is consistent with the long-held axiom among Astronomers and Planetary Scientists that 'silicate' dust in the Galaxy initially formed by vapor-to-solid condensation in cooling O-rich circumstellar atmospheres as well as in the 4.6 Ga-old solar nebula [3,4].

It is relevant then to ask if we could predict the chemical and crystallographic properties of these metastable solids? As an initial approach, we use binary phase diagrams with multiple eutectic points to explore the compositions of the metastable eutectics. These compositions will not match any thermodynamically stable stoichiometric minerals. The metastable eutectic solids with predictable chemically ordered compositions will be amorphous. Thus, they will contain a considerable amount of "internal chemical and crystallographic free energy". As a result there is little activation energy required to start seemingly chaotic sequences of kinetically controlled reactions that may ultimately reach thermodynamic equilibrium.

Metastable eutectic solids may exist in many environments from natural and anthropogenic processes. It is possible that predictable metastable behavior may be a very common phenomenon but one that we have yet to recognize. We submit that the boundary conditions that lead to metastable eutectic behavior will be both high temperatures and ultra rapid quenching. What geological environments or processes meet these boundary conditions? Such environments are not necessarily unique to the Earth and should therefore exist on other terrestrial planets and satellites in our solar system. Anthropogenic processes leading to metastable eutectic behavior include coal burning and nuclear waste storage and disposal.

In this paper we report the properties of chemically ordered solids at metastable eutectics that were obtained during systematic gas-to-solid condensation experiments of three binary vapors and one ternary metal-oxide vapor. We will investigate the occurrence of metastable eutectic behavior in selected natural and anthropogenic environments and processes but this paper is admittedly an incomplete survey of the available literature. We will highlight the possibilities and implications of metastable eutectic behavior whenever the right physical conditions of high temperature and ultra-rapid quenching occurs. This particular non-equilibrium behavior offers as yet unexplored exciting and new research opportunities in Earth and Planetary Sciences with implications we still have to fully appreciate as well as in many other areas and we invite readers to explore the applicability of predictable metastable equilibrium.

## GAS-TO-SOLID CONDENSATION EXPERIMENTS

### The Condensation Experiments

The samples were produced by non-equilibrium gas-to-solid condensation using the Condensation Flow Apparatus described by [4,5]. In this apparatus there is no standard set of flow, temperature or pressure settings, but the following conditions are all at least somewhat typical of an average experiment. The total pressure in the system is ~100 torr while the temperature in the furnace is ~1000K. The hydrogen flow rate is ~1000 sccm (standard cubic centimeters per minute). The helium flow through the iron-carbonyl is on the order of 500 sccm. We estimate that the iron carbonyl concentration is ~10% of the total flow of helium. Magnesium metal is placed into a graphite boat inside the furnace. At the nominal 1000K temperature of the furnace, magnesium metal has a vapor pressure of ~5 torr. The oxygen flow rate always equals or exceeds that of silane ($SiH_4$) but is usually within a factor of two of the silane setting. The silane flow rate is typically ~100 sccm. The hydrogen to oxygen ratio is always >5 as some amount of hydrogen is also contributed by silane. The typical oxygen flow is sufficient to just balance hydrogen contributed from the silane flow to produce water and $Si^0$ without effecting the bulk flow of hydrogen. The amount of hydrogen in the system was insufficient to cause the hydration of the ~20 nm-sized solids at a nominal quenched temperature of 775K even though hydrogen was the dominant gas present in the system. It is possible that $Si_2O_3$ condenses in a complex vapor [6]. The amount of water during condensation might then be controlled by the reaction $Si_2O_3 + H_2O = 2\ SiO_2 + H_2$. Some of level of 'juvenile' hydration might occur in the experiments but the formation of layer silicates in condensed samples typically requires substantial time, temperature and water-saturated conditions [7,8].

In this system the oxygen fugacity is a dynamic quantity that is dependent on reaction rates, rather than a thermodynamic quantity. The actual oxygen fugacity during condensation is conducive to formation of iron oxides instead of $Fe^0$, to the formation of silicon oxides instead of $Si^0$, and formation of magnesium oxides rather than Mg metal. Details of the condensation experiments are available for the Al–SiO-$H_2$-$O_2$ [9] (Fig. 1), Mg-Fe-SiO-$H_2$-$O_2$ [10], Fe-SiO-$H_2$-$O_2$ [11], Mg-SiO-$H_2$-$O_2$ [4] vapors. The bulk compositions of the condensing gases are unknown. They will be close to the bulk composition of the average solid, which can be obtained analytically by grain-by-grain analyses in the analytical electron microscope (AEM) [10] or via low resolution SEM studies of pressed powder samples.

### Electron Microscope Analyses

A small portion of the condensed material from each experiment was embedded in epoxy (Spurrs) to prepare serial ultrathin sections (90 nm thick) using a Reichert-Jung Ultramicrotome E equipped with a diamond knife. The ultrathin sections that are transparent to the electron beam were placed on holey carbon thin-films supported by standard 200 mesh Cu grids for study in a JEOL 2000FX transmission electron microscope (TEM). The microscope operated at an accelerating voltage of 200 keV and was equipped with a Tracor-Northern TN-5500 energy-dispersive spectrometer (EDS) for analysis of elements with atomic number >11. The analytical spot size was ~10-20 nm in diameter. Quantitative determination of the composition of individual grains >10 nm in diameter was obtained by the Cliff-Lorimer [12] thin-film correction procedure. The error in abundances of major-element oxides is 5% relative. Artifacts in grain composition could arise from overlapping grains smaller than the section thickness. This potential artifact was not a problem in this ATEM study. Prior to analysis each grain was viewed using a "through-focus" technique to determine the possible presence of additional grains along the electron beam's path. The location of each EDS analysis was recorded on TEM micrographs to evaluate possible contamination. Imaging in the TEM viewing mode is routinely possible with a 0.2-nm spatial resolution. The dimensions of condensed solids were measured in calibrated TEM micrographs with a 10% relative error. The crystallographic grain properties, *i.e.* amorphous or crystalline, were determined by selected-area electron diffraction whereby relative errors in the interplanar (*d*-) spacings are 2% relative for single-crystal grains; ~10% relative for small grain clusters based on polycrystalline (or "ring") patterns.

## PREDICTABLE METASTABLE EUTECTICS: CONDENSATION EXPERIMENTS

### General results

The nanometer-sized condensates are

1. crystalline end-members, *viz.* $Fe_3O_4$ (magnetite), $\gamma$-$Fe_2O_3$ (maghémite) and MgO (periclase),
2. amorphous mixed metal-oxide/silica solids with intermediate compositions, and
3. abundant tridymite, a high-temperature $SiO_2$ polymorph, that may contain small amounts of Fe, Mg, or Al.

The most amazing finding is that compositional groupings of the invariably amorphous mixed metal-oxide/silica solids match metastable eutectics in the appropriate binary phase diagram.

During the waning of the condensation phase proper, the solids are subject to post-condensation adjustments when the thermal energy of condensed solids is still high. We found spinodal decomposition in metastable eutectic ferrosilica solids (see Fig. 3 in ref. [11]). Crystallization of the initially amorphous condensed end-member solids could also be a post-condensation, *i.e.* autoannealing feature. Heat treatment at 1000K for 4 hours in vacuo caused a solid-state amorphization transformation of compact polycrystalline tridymite aggregates (Fig. 2) into amorphous silica spheres (Fig. 3) that are thermodynamically unstable.

**The $Al_2O_3$-$SiO_2$ system: Kinetic effects**

Polymerization of silica melts by alumina introduces spurious kinetic effects in quench-melt experiments to determine the liquidus topology of the $Al_2O_3$-$SiO_2$ phase diagram. At issue is the nature of *mullite* melting. Consequently there are two accepted versions of this equilibrium phase diagram in use today. Each diagram has one metastable eutectic point but at a different composition (Fig. 4). The condensed intermediate amorphous aluminosilica solids had compositional peaks at 11.5 and 47-wt % $Al_2O_3$ each matching a metastable eutectic in one of these two diagrams but at different composition (Table 1). Another group of condensed aluminosilica solids is clustered at 7-wt % $Al_2O_3$ and the solids have a distinct crystalline rim [see Fig. 3 in 9]. In the original data reduction these rimmed grains were treated as a group separate from the amorphous aluminosilica solids [9]. It is possible that they might be affiliated with the metastable eutectic solids at 11.5-wt % $Al_2O_3$. In that case, it remains to be explained why they are texturally different. Kinetic affects caused by rapid polymerization of the vapor by alumina at the molecular level may have affected vapor phase condensation. Pure $Al_2O_3$ grains did not condense: this may be related to the fact that corundum is a poor glass-former. Amorphous alumina exists only at liquid He temperatures. Assuming that initially amorphous end-member oxides became ordered only during post-condensation autoannealing, it appears that condensation of ordered alumina (*corundum*) is a unique equilibrium phenomenon, or is restricted to extremely cold astrophysical environments.

**The $FeO/Fe_2O_3$-$SiO_2$ system: *Oxygen fugacity***

Oxygen fugacity is an important parameter in Fe-containing systems. In the experiments reported here, the oxygen fugacity varied randomly during gas-to-solid condensation. When both ferrous and ferric iron vary during condensation, the (pseudo) binary system $FeO/Fe_2O_3$-$SiO_2$ has

three metastable eutectics (Fig. 5). The iron content of the condensates is thus presented as 'FeO' without consideration of the actual $FeO/Fe_2O_3$ ratio unless mineralogical data is available to make an appropriate identification. The ferrosilica condensates had three compositional peaks, *viz.* at 97, 33 and 17-wt % 'FeO' (Table 1). Almost pure Fe-oxide defines a Si-bearing maghémite metastable eutectic at 97-wt % $Fe_2O_3$ [11]. The compositions of the other metastable eutectics vary as a function of the $FeO/Fe_2O_3$ ratio. The composition is 17-wt % 'FeO' for $FeO/Fe_2O_3 = 8/2$ whereas this composition is 33-wt % 'FeO' when $FeO/Fe_2O_3 = 6/4$ [11]. During non-equilibrium condensation the ferrosilica grains typically occur at both intermediate metastable eutectics. The Fe/Si ratio of the metastable eutectic at 17-wt % 'FeO' does not match the Fe/Si ratio of naturally occurring minerals. However, the solids ordered at the 33-wt % 'FeO' metastable eutectic have the same Fe/Si ratio as Fe-saponite, a smectite group mineral. This condensation experiment clearly demonstrated that oxygen fugacity remains a defining parameter when establishing predictable metastable equilibrium in Fe-bearing vapors. Unfortunately, because of the dynamic nature of the processes leading to metastable eutectic equilibrium, it may never be possible to completely control or predict the oxygen fugacity at the point of condensation.

## The $MgO-SiO_2$ System

The magnesiosilica solids condensed in a $Mg-SiO-H_2-O_2$ showed chemical ordering at two compositional peaks, 28 and 50-wt % MgO, that match the metastable eutectics in the $MgO-SiO_2$ binary phase diagram (Fig. 6). These solids define two distinct metastable eutectics, *viz.* (1) serpentine-dehydroxylate, $Mg_3Si_2O_7$, and (2) smectite dehydroxylate, $Mg_6Si_8O_{22}$ (Table 1). The dehydroxylate Mg/Si ratios are the same as the layer silicate minerals serpentine and smectite (saponite) or talc.

## The $MgO-FeO/Fe_2O_3-SiO_2$ system

To explore how metastable eutectic behavior affects the condensed solid compositions in ternary oxide vapors, we studied the condensates from a $Mg-Fe-SiO-H_2-O_2$ vapor. The (pseudo) ternary $MgO-FeO/Fe_2O_3-SiO_2$ diagram is of considerable interest because it includes several common rock-forming minerals, *viz.* olivine, pyroxene and several layer silicate minerals (Table 2). The condensed magnesiosilica and ferrosilica solid compositions faithfully mimicked the metastable eutectics in the individual binary systems (Figs. 5,6); metastable eutectics occurred at 50 and 28-wt % MgO, 97-wt % $Fe_2O_3$, and 33 and 17-wt % 'FeO' (Table 1). This particular non-

equilibrium gas-to-solid condensation experiment revealed some phenomena with possibly far-reaching implications. The experiments showed that

1. There were no condensed solids on the MgO-FeO/$Fe_2O_3$ join, which is consistent with complete solid solution in the Mg-Fe and MgO-FeO/$Fe_2O_3$ binary systems [10]. This 'negative' result confirms metastable eutectic behavior at predictable compositions, and that metastability is an essential component of condensing clusters,
2. Condensation did not yield solids with a mixed ferromagnesiosilica composition (Fig. 7),
3. Ferrosilica solids were also ordered at the predicted greenalite dehydroxylate metastable eutectic, $Fe_3Si_2O_7$ (Figs. 5, 7), with the same Fe/Si as greenalite, $Fe_3Si_2O_5(OH)_4$ (Table 2). This metastable eutectic at 70-wt % FeO replaces the intermediate 'FeO' metastable eutectics (Table 1) when ferrous iron is the predominant iron species in the vapor [10].

### Implications

Predictable metastable eutectic behavior is not just a theoretical oddity. One of the fascinating facts is that this chemical ordering of metal/Si ratios at metastable eutectics resembles the ratios of layer silicates (Table 2) which we will discuss below. Metastable eutectic solids will contain considerable "internal chemical and crystallographic (being amorphous) free energy". They require little activation energy to start a seemingly unpredictable sequence of kinetically controlled reactions that will lead to thermodynamic equilibrium. Any intermediary phases are likely to include ultrafine-grained stoichiometric minerals that form outside their thermodynamic stability fields. The non-equilibrium condensation experiments showed that the conditions needed for predictable chemical ordering at metastable eutectics are high temperature and (ultra) rapid quenching. Similar conditions may characterize other processes and it is possible that this type of predictable non-equilibrium may be a common feature in many extraterrestrial and terrestrial environments, albeit one that we have yet to recognize.

## EXTRATERRESTRIAL ENVIRONMENTS

### O-rich circumstellar dust

The identification of silicates in dusty astrophysical environments relies on *infrared (IR) spectroscopy* [4,5]. The strength and exact positions of the 10 μm and 20 μm IR spectral features related to the Si-O stretching and O-Si-O bending modes are diagnostic to determine the nature of

these silicates and their aging properties [3,13]. In combination with reasonable assumptions concerning the *cosmic elemental abundances*, the IR data were interpreted as amorphous Mg-rich 'olivine' dust, 'disordered olivine' [14] and fully-ordered forsterite with small amounts of Na, Ca, and Al [15]. The silicate mineralogy might be more complex and could also include amorphous and crystalline Mg,Fe-pyroxenes [16,17] and plagioclase ($Ca_2Al_2Si_2O_8$) [18]. Whether this range of mineral and structural properties is real, an artifact of IR spectral resolution and date reduction, or both, is not clear. The *Infrared Astronomical Satellite* observations at mid-infrared wavelengths [19] showed relatively little variation in the spectral properties of dust around a very wide range of stellar sources. Until the amazing observations made by the *Infrared Space Observatory* (*ISO*) satellite [20,21] most researchers believed that all such condensates were amorphous and that compositional data would be impossible to derive from these observations alone. However, *ISO* observations at far-infrared wavelengths showed that in certain relatively rare, high-mass-loss-rate stellar outflows, nearly pure magnesiosilica grains form and anneal to crystalline Mg-silicates without detectable iron. Despite copious quantities of amorphous dust crystalline Fe-silicates have not yet been observed in such sources. A dearth of crystalline Fe-silicates could be explained by the experimentally obtained result that magnesiosilica solids anneal much more rapidly than do ferrosilica condensates [22].

Only condensation at metastable eutectic compositions can explain the formation of pure Mg-SiO dust in the form of chemically ordered amorphous $Mg_3Si_2O_7$ and $Mg_6Si_8O_{22}$ grains (Fig. 6). These grains will thermally anneal to crystalline phases in the high temperature environments of these massive stellar outflows. In less massive outflows none of the grains experience temperatures high enough to induce crystallization and all condensates therefore remain amorphous. The hypothesis that condensation occurs at metastable eutectic compositions does bring order to an otherwise chaotic situation because it limits the number of different possible thermodynamic equilibrium condensates to a finite set of ferrosilica, magnesiosilica and simple metal-oxide grains no matter the bulk composition in various O-rich circumstellar environments. Wide variations in stellar composition can easily be accommodated by changes in the relative proportions of the metastable condensates.

Within limits the compositions of minerals formed after thermal annealing are also predictable using nucleation theory and bulk chemistry [23] and some consideration of the surface free energy of the system [24,25]. For example, thermal annealing of serpentine dehydroxylate (Fig. 6) ideally yields olivine + pyroxene, *viz.* $Mg_3Si_2O_7 \Rightarrow Mg_2SiO_4 + MgSiO_3$ wherein the reaction products will be ultrafine-grained thermodynamically unstable minerals. Instead, experimental studies show that the reaction, $2\ Mg_3Si_2O_7 \Rightarrow 3\ Mg_2SiO_4 + SiO_2$, produces a thermodynamically

unstable assemblage of forsterite + tridymite before reacting to form enstatite + forsterite during continued heat treatment, *viz.* 3 $Mg_2SiO_4$ = 2 $Mg_2SiO_4$ + $Mg_2Si_2O_6$. The thermodynamically unstable assemblage exists because of the surface free energy of the phases [24].

## Solar nebula dust

The dust in astrophysical environments is only accessible by remote sensing observations and laboratory simulation studies [4,26]. This situation is much improved for our own solar system because the collected meteorites, micrometeorites [27,28] and interplanetary dust particles (IDPs) are samples from protoplanets that still exist as small solar system bodies. The protoplanets include a wide variety of *asteroids* such as near-Earth Asteroids and those in the asteroid belt between Mars and Jupiter [29] and comet nuclei from the *Kuiper belt* and the *Oort cloud* [30,31]. The distinction between asteroids and comets is not always unambiguous. For the present purpose comet nuclei are 'dirty-ice' balls or rubble piles thereof [32] while asteroids are compacted ice-free bodies that experienced variable levels of aqueous or thermal alteration, or some combination of both. Protoplanets contain information on the dust from which the solar system formed (presolar dust) and the dust that condensed from the cooling solar nebula gas phase (solar system dust).

The carbonaceous chondrite meteorites represent the least modified asteroids. For example, the elemental abundances of CI-type carbonaceous chondrites are identical to those of the solar photosphere except for the most volatile elements, such as C, H, O, N [33]. Solar or cosmic elemental abundances are a primitive chemical signature [34] of materials that did not experience post-accretion alteration. Somewhat surprisingly because the collected *CI carbonaceous chondrites* are fully hydrated and contain veins of salt minerals that indicate open-system chemical transport and possible loss of volatile and soluble elements at an early stage of during their evolution [35]. Yet, they are considered to be representative of the solar or cosmic elemental abundances but the abundance of a soluble element such as sodium is probably depleted in the CI carbonaceous chondrites. In fact, the compositions of anhydrous cluster IDPs indicate a higher Na abundance of 2 x CI [36].

## Equilibrium condensation

The *molecular cloud* wherein our Sun was formed contained dust condensed in and ejected from O-rich stars. This dust was present throughout the solar nebula surrounding the Sun and the Giant Molecular Cloud core. During the highly energetic *T-Tauri phase* in the evolution of the

sun this dust was completely evaporated in a region close to the star. Similarly, viscous dissipation of the angular momentum of infalling material also caused vaporization of even the most refractory materials in some regions [37]. This vapor condensed in cooler regions at greater distances from the sun. The size of this zone of evaporation and condensation is not exactly known but its greatest extent was probably within Jupiter's orbit. Beyond Jupiter the original presolar dust generally survived and was incorporated into the protoplanets that became comet nuclei. It was generally assumed that all mineral constituents of the unequilibrated chondrite meteorites that include the carbonaceous chondrites are thermodynamically stable phases. This situation has led to a model of equilibrium condensation of stoichiometric thermodynamic phases in a cooling solar nebula gas of chondritic composition.

For almost forty years equilibrium condensation models have been used to predict the stoichiometric minerals that form in a cooling solar nebula. Equilibrium condensation began with corundum ($Al_2O_3$) at ~1680K followed by $CaTiO_3$ (perovskite) and $Ca_2Al_2SiO_7$ (gehlenite) at ~1575K, then $Ca_2MgSi_2O_7$ (åkermanite), $MgAl_2O_4$ (spinel), diopside and metallic iron between ~1350-1400K. Next form forsterite ($Mg_2SiO_4$), enstatite ($MgSiO_3$), plagioclase, alkali-feldspars [$(K,Na)AlSi_3O_8$], and magnetite between ~1475-1100K. Finally, layer-silicates form via hydration of previously condensed silicates below ~400K [38,39]. This condensation sequence is an unlikely natural process. For example, the reaction $[Mg_2SiO_4]_{(gas)} \Rightarrow [Mg_2SiO_4]_{(solid)}$ is impossible as written because there is no forsterite gas molecule. The formation of forsterite and other 'complex" stoichiometric silicate minerals requires unique conditions which are not conducive to widespread silicate condensation. Numerous petrologic studies of meteorites have yet to produce unambiguous evidence for fractional equilibrium condensation. In preceding sections we discussed that, for example, olivine crystals cannot be original condensates but must be secondary phases formed following condensation and aggregation of primitive condensates and after considerable heat treatment. The collected aggregate IDPs are the most pristine, *i.e.* least-altered or modified, samples from the earliest epoch of our solar system that are available to laboratory analyses. These IDPs could still contain the remnants of the circumstellar dust types that were formed by vapor phase condensation. There is a steady influx of IDPs to the Earth's atmosphere. They can be considered the shooting stars that survived atmospheric entry heating during deceleration in the atmosphere at altitudes between 100-80-km.

## Chondritic aggregate IDPs, or cosmic dust

Briefly, IDPs are collected in the Earth's stratosphere between 17-19-km altitudes using flat-plate collectors mounted underneath the wings of high-flying aircraft. Details are available on the collection and curation [40], the mineralogy, major and minor element compositions [30,31,41], the isotopic compositions [42], and physical properties [43,44]. The 10-50-μm-sized aggregate IDPs, that are a subset of the collected stratospheric particles, have close-to-chondritic bulk compositions although none of their individual constituents has a chondritic composition [30] (Fig. 8). The IDPs include the solid debris of comets released during the sublimation of water ice at the nucleus surface [45] and primitive asteroids where they are probably released during impact by a smaller body and/or during catastrophic disruption.

The sizes and compositions of dust analyzed near the nucleus of comet Halley [46] show considerable similarities with the matrix constituents in aggregate IDPs [10,30,31]. We note that the current Stardust Mission to comet P/Wild should eventually yield samples from a second comet. These similarities forge a reasonable link between cometary dust and aggregate IDPs that contain remnants of presolar dust. This link offers some interesting insights for interpretation of the IR spectra of interstellar and cometary dust. For example, plagioclase could be an equilibrium phase according to equilibrium condensation models [38] among circumstellar dust [18]. Taking the relative cosmic elemental abundances [34] into account, Ca±(K,Na)-bearing aluminosilica phases will be less abundant than ferromagnesiosilica dust. The petrologic relationships of rare plagioclase and alkali-feldspar in aggregate IDPs show a secondary, not a condensation, origin [30,41]. It seems unlikely that in the absence of significant post-condensation thermal annealing plagioclase can be abundant among the circumstellar dust.

The matrix of an aggregate IDP is by itself an aggregate of three distinct spherical units or Principal Components (PCs) [30,31] including two chemically and texturally different (C-free) ferromagnesiosilica PCs that range from ~90 nm up to 2-3 micrometer in diameter, viz.

1. Coarse-grained smectite dehydroxylate, $(Mg,Fe)_6Si_8O_{22}$, units with Fe/(Fe+Mg) (*fe*) = 0 – 0.36 (element ratio), and
2. Ultrafine-grained units with a serpentine dehydroxylate, $(Mg,Fe)_3Si_2O_7$, composition and *fe* = 0.36 – 0.83 identical to the ferromagnesiosilica [47] units of glass with embedded metals and sulfides [48].

The minerals observed in these PCs are secondary phases that were formed in an originally amorphous material [30,31] whereby the coarse-grained units are probably the result of fusion (i.e. compaction) of ferromagnesiosilica aggregates consisting of condensed ferrosilica and magnesiosilica dusts [10]. This model is based on the results of the Mg-Fe-SiO-$H_2$-$O_2$ vapor condensation experiments. That is, the proximity of the condensed amorphous metastable eutectic

and end-member solids in this ternary system offered the opportunity for mixing along tie lines connecting the condensed solid compositions. In this manner, the chemically reactive solids will be able form ferromagnesiosilica aggregates that, given the opportunity, could become fused into homogeneous amorphous ferromagnesiosilica grains. In environments dominated by gas-to-solid condensation aggregation will be the only way to obtain mixed ferromagnesiosilica grains with predictable metastable mixed ferromagnesiosilica compositions. This is shown in Fig. 9 where three randomly selected bulk compositions of these coarse-grained PCs are uniquely defined by the tie lines connecting the condensed solid compositions [10,30]. The high degree of chemical order is one of the most remarkable properties of chondritic aggregate IDPs and is consistent with predictable non-equilibrium condensation in O-rich circumstellar atmospheres.

**Shock metamorphism: Impact structures and simulation experiments**

Hypervelocity impacts are an important process in the evolution of the solar system [49,50]. The resulting impact structures can show a wide range of shock metamorphic features ranging from unique dislocation microstructures in minerals, melting, and melt-vein intrusion to evaporation [51]. Apart from Lunar craters sampled during the Apollo program, the only impact structures that are accessible to laboratory analyses are those that survived in the geological record. We selected two examples to explore metastable eutectic behavior in the kinetically controlled environment of impact events.

The first example is the 23 Ma-old Haughton crater (Canada) wherein the crustal rocks experienced impact-induced phase transformation at peak pressures between 50-60 GPa (1 GPa = 10 kbar) [52]. This well-documented petrologic study of shock metamorphism describes several mineralogical domains in shocked *gneiss* fragments from the allochthonous *polymict breccia* in this crater. One newly formed amorphous region was reported as having "a rather homogeneous composition with a very peculiar Al/Si ratio close to 1. Such a ratio is inconsistent with the chemistry of any pre-shock mineral in the sample." [52]. The average composition of this amorphous material is $SiO_2$ = 58-wt % and $Al_2O_3$ = 42-wt %. This material and amorphous material associated with shocked feldspars contain needles of an unknown $Al_2O_3$ polymorph. Shock-produced *coesite*, *cristobalite* and amorphous $SiO_2$ occur in addition to pre-shock quartz, and euhedral mullite crystals surrounded by $SiO_2$–rich glass [52]. These and other petrologic features in the shocked gneiss fragments were thought to have formed in response to very fast local equilibrium reactions during shock-induced temperatures of 1675K, and locally up to 2775K, and thermal decay at moderate to low pressures to ~1475K in a few milliseconds [52].

The unique shock-produced amorphous aluminosilica material has a metastable kaolinite dehydroxylate composition (Table 1). An alternative scenario accepts the existence of domains of metastable eutectic equilibrium rather than pervasive equilibrium in this impact structure. That is, formation of amorphous kaolinite-dehydroxylate material, which during post-shock thermal annealing was decomposed into mullite surrounded by $SiO_2$ glass, *viz.* $3\ Al_2Si_2O_7 = Al_6Si_2O_{13} + 4\ SiO_2$. The submicrometer mullite may not be a thermodynamically stable phase. Nanometer-sized $Al_2O_3$ needles in the amorphous aluminosilica material might share a similar annealing history. The physical conditions during shock-impact metamorphism will be conducive to metastable eutectic behavior. Consequently there should be some reservation to assign thermodynamic equilibrium to the submicrometer-sized phases.

This observation leads to experimental studies of impact-shock metamorphism. To illustrate this point, we selected a study on disequilibrium features in experimentally shocked powders of mixed olivine and silica glass that are chemically incompatible and coexist only in metastable equilibrium below 1475K at 1 atm. pressure [53]. The composition of shock-produced pale to dark green Mg-rich ferromagnesiosilica melts did not vary as a function of shock pressure between 42.9 and 62.2 GPa. But, "Surprisingly, the compositions of the colored glasses are intermediate between the composition of pure olivine [that was used as a starting material, our comment] and the bulk composition of the original starting material (79-wt % $SiO_2$) and are similar to enstatitic pyroxene compositions" [53]. There was no evidence for the presence of this pyroxene in the starting and shock-produced materials and thus it was suggested that the melt compositions might indicate "an incipient eutectic-type fusion" [53]. The recalculated melt compositions [Table 2 in 53] are clustered mostly at the intersection of a tie line connecting the starting material and original olivine compositions with one of the metastable eutectic mixing lines in the Mg-Fe-Si diagram (Fig. 10). The melt composition at 61.0 GPa that falls below the tie line might indicate loss of iron and Si-enrichment but no data are available to assess this possibility, or the possibility of melt heterogeneity. The "incipient eutectic-type fusion" in this experiment might be equivalent to predictable metastable eutectic non-equilibrium behavior.

## TERRESTRIAL ENVIRONMENTS

Most ordinary rocks do not appear to contain phases with metastable eutectic compositions although the appropriate boundary conditions might exist in many terrestrial environments. One such example is pyrometamorphic buchites resulting from underground coal fires. They are something of a petrologic oddity containing unusual $Fe^{3+}$-rich minerals and characterized by

millimeter-scale mixing of equilibrium minerals and non-equilibrium domains [54,55,56]. It is possible that these non-equilibrium domains might represent metastable eutectic equilibrium.

Fulgurites, another petrologic oddity, form when a lighting strike hits the Earth's solid surface. Because many surface materials such as soils contain organic materials, interactions with a lightning strike cause extreme reduction at air temperatures up to ~30,200K leading to the formation of metallic phases that are not normally found at the surface [57]. Fulgurites are amenable to experimental study using triggered-lightning strikes. In a recent experiment, wherein the oxygen fugacity was not buffered, a lightning strike penetrated a stack of alternating slabs of magnetite and aluminosilica glass wool (42-wt % $SiO_2$; 58-wt % $Al_2O_3$) producing various ferroaluminosilica phases [58]. The compositions (~40-wt % $Al_2O_3$) of neoformed aluminosilica glass spheres match the metastable kaolinite dehydroxylate eutectic (Table 1). Lightning produced $Fe^{3+}$-rich cordierite glass, $Al_{2.1}{}^{3+}Fe_{0.9}{}^{2+}Fe_{1.8}(Al_{0.6}Si_{5.4}O_{18})$. Applying the criteria for chemical ordering at metastable eutectics to the FeO-$Al_2O_3$ phase diagram [59], we predict a metastable eutectic point at ~35-wt % $Al_2O_3$. The unique $Al_2O_3$.FeO.$Fe_2O_3$ spinel dendrites, FeO/$Fe_2O_3$ = 8/2, that grew rapidly in the glass during thermal recovery (autoannealing) might represent metastable eutectic behavior. This experiment showed a mixture of predictable metastable eutectic and equilibrium phases [58] similar to the observations of coal-fire buchites.

**Volcanic ash**

Micrometer-sized and smaller dust in Plinian-type volcanic eruption plumes, such as the Mt. St. Helens, El Chichón and Mt. Pinatubo volcanoes, could have metastable eutectic compositions. This dust is dispersed by aeolian transport in the troposphere and when carried aloft in ejecta plumes directly into the stratosphere its dispersal will be on a global (hemispherical) scale. A limited literature survey showed that aluminosilica shards and aggregates with <10 wt % other elements (mostly Fe, Ti, Ca, K or Na) are common among volcanic ash. For example, in the Antarctic [60] and Greenland [61,62] ice sheets, in the stratosphere at ~35-km altitude [63], and among shards and spheres in the Mt. Etna volcanic plume [64,65]. The shards are angular with a smooth surface. The $Al_2O_3$ content of this glassy and tridymite-rich [66] volcanic dust defines a trimodal distribution (Table 3).

The micrometer-sized airborne coal-burning dust emissions in the Upper Silesian Industrial Region (USIR) of Poland lack the typically abundant fly ash spheres. It include a high abundance of ~0.1 to ~5.2 micrometer-sized pure silica and aluminosilica shards and clusters, and only rare silica spheres (Fig. 11). The mostly compact grains have a smooth surface. The log-normal size

distributions of the shards and the presence of clusters suggested that this dust is volcanic ash that survived inefficient coal burning for domestic use [67]. In other words, the low-temperatures in domestic furnaces hardly modified this volcanic ash from the time of coal deposition. This observation was the first to recognize fossil volcanic dust among coal fly ash although it is well documented that natural coals typically contain mineral impurities such as quartz, feldspars, layer silicates including mica and illite, $Al_4Si_8O_{20}(OH)_4$ and sulfides.

A comprehensive long-term study of airborne coal-burning emission in USIR found massive and porous glassy aluminosilica shards with two discrete size ranges from 19 up to 27 and 37 up to 55 micrometer, and abundant spheres ranging from 2 to 55 micrometer [68] (Table 3). The grains belonging to the population with mean $Al_2O_3$ = 22.6 wt % have similar sizes as the dust collected during 1994 June [67] but they are not smooth angular shards [68]. The surface appears to be etched and many aluminosilica grains show a three-dimensional skeletal framework giving them an almost spongy appearance (Fig. 12). A few compact grains have a spongy rim. Large grains still have an angular outline but the smallest grains have lost any vestiges of sharp edges. Rare spheres also belong to the compositional group of skeletal aluminosilica grains with the formula $Al_4Si_8O_{22}$ and the same Al/Si ratio the clay minerals pyrophyllite and illite. Some fraction of the amorphous aluminosilica grains in the population with mean = 11.5 wt % $Al_2O_3$ also have a skeletal or spongy texture and their average composition is close to $Al_2O_3 \cdot 12SiO_2$.

The compositions of spongy aluminosilica grains match the thermally annealed metastable eutectic, $Al_2O_3 = 26.6 \pm 4.4$, on the low-alumina limb of the spinodal solvus in the $Al_2O_3$-$SiO_2$ phase diagram [9]. It supports a scenario wherein fossil, metastable eutectic, volcanic dust with $Al_2O_3 = 12.4 \pm 2.7$ was heated sufficiently during coal combustion to initiate decomposition, *viz.* $2\ Al_2O_3 \cdot 12SiO_2 = Al_4Si_8O_{22} + 16\ SiO_2$, with the resulting aluminosilica composition on the spinodal solvus. Silica vapor condensation could have produced the tiny hollow [58] nanometer-sized silica spheres. The predictable metastable compositions, the textures and morphologies, of the airborne aluminosilica dust grains are consistent with thermal annealing and partial evaporation during burning of fossil volcanic dust impurities in locally used coals

**Coal fly ash**

Industrial coal burning produces aluminosilica spheres, and aggregates of spheres, with iron oxides, MgO, CaO and $K_2O$ as other major components; less commonly, aluminosilica spheres can have <10-wt% other elements [69,70,71,72]. The spheres can be massive, frothy (or spongy) or hollow in which case they may be filled with many smaller spheres [72,73]. Massive spheres

can be glassy or partially devitrified with randomly oriented mullite needles in an amorphous aluminosilica matrix [69,70,73]. The compositions of almost pure aluminosilica spheres closely match with the kaolinite dehydroxylate metastable eutectic composition (Table 4). Two coal fly ash spheres (18.3 and 29.3-wt % $Al_2O_3$) match the formula $Al_4Si_8O_{22}$ of the pyrophyllite or illite dehydroxylate composition of the spongy (frothy) fly ash grains collected in USIR. Isolated coal fly ash spheres were rare among the finest collected dust [67] but massive glassy aluminosilica spheres were common in aggregate particles in USIR (Fig. 13). These aluminosilica spheres typically contain more than 10-wt % but <35-wt % Fe-oxides, $K_2O$, $Na_2O$, CaO, MgO or $TiO_2$whereby Fe and K are the most abundant elements present [68]. In addition Zn, Mn or Cu are present in spheres with highest content of other elements. Fewer than 2% of all spheres are aluminosilica with <10-wt % other elements [68] with $Al_2O_3$ contents displaying tri-modal distribution (Table 4). The spheres with mean = 8.2-wt % $Al_2O_3$ are 15% of all aluminosilica spheres with <10-wt % other elements.

## RESEARCH OPPORTUNITIES

### Interplanetary Dust Particles

Thermal events that will be conducive to metastable eutectic behavior in aggregate IDPs are

1. Irradiation by energetic H and He atoms and interactions with solar flares in space [48], and
2. Dynamic pyrometamorphism during atmospheric entry [30,41].

Single crystals embedded in aggregate IDPs, such as Mg-rich olivine, enstatite and diopside can develop amorphous rims or become almost completely amorphous when they were exposed to the space radiation environment. These interactions may cause Mg-loss and O-enrichments leading to non-stoichiometric amorphous materials [23,30,48,74]. These radiation-induced compositions resemble serpentine and Si-rich smectite metastable eutectic dehydroxylates [23,74]. Possible effects of dynamic pyrometamorphism to the observed non-stoichiometry are undefined but radiation-induced non-stoichiometry and structural defects will undoubtedly facilitate thermal modification. Flash-heating alteration in IDPs is a largely unexplored area of research.

### Environmental Mineralogy

Air-borne dusts in our respiratory system, soils and surface-waters become potential health hazards. The properties that determine the dust interactions in these environments such as the level of biological activity in the human lungs [75] include:

1. The size and shape of the grains,
2. Crystallochemical properties of the crystalline phases,
3. Their amorphous, disordered or fully-ordered nature,
4. Surface chemistry, topography and electrical charge, and
5. Associates trace phases.

This listing does not specifically include the surface free energy for nanometer-sized dust or the Gibbs adsorption isotherm that drives chemical impurities to the surface of liquids to lower the surface free energy. It also does not consider the "internal free energy" of metastable eutectic dust. The emerging sub-discipline of Environmental Mineralogy should carefully consider the role of metastable eutectic dusts. For example, chrysotile, $Mg_3Si_2O_5(OH)_4$, asbestos can make up more than 50% of the fibrous-mineral lung burden [76]. It has become increasingly clear that this particular form of asbestos is much less dangerous than crocidolite because chrysotile is highly soluble in the lung environment [75]. Conceivably this behavior is in part related to the serpentine-dehydroxylate chemistry. In general, inhaled dust with metastable eutectic compositions should be more soluble than equilibrium mineral dust.

**Metamorphic reactions**

In a preceding section we discussed shock metamorphism in a terrestrial impact structure. Similar processes have defined the formation and evolution of the regolith at both the lunar and asteroidal surfaces. Samples of asteroidal regolith breccias show evidence for localized shock melting. We predict that these melts display metastable eutectic behavior. Indeed, interstitial aluminosilica (with <10-wt % other elements) melts in two H-chondrites, Nulles and Dimmitt, have 16.2 and 25.1-wt % $Al_2O_3$ and 19.4 and 20.7-wt % $Al_2O_3$, respectively [77] that match the metastable aluminosilica eutectics (Fig. 4).

Regional and contact metamorphism both take place gradually over periods of millions of years whereby one equilibrium mineral assemblage transforms into a new assemblage that is in thermodynamic equilibrium at the new PT conditions. The transition is probably characterized by a series of kinetically controlled reactions. It is possible that the ensuing chain of metamorphic reactions could proceed in a predictable manner. The properties of these reactions might be

hidden in a "black box" of metastable intermediates in reactions such as A + B = "black box" = C + D.

High-resolution TEM studies of the mineralogical interrelationships observed during mineral reactions have revealed complex behavior at the unit cell level. Reaction zones are often lamellar or interstratified microstructures of starting and reaction products. Biopyriboles [78,79], among many others) are an example of an interlayered 'intermediate microstructure'. The formation of new interfaces is costly and adds surface free energy to the assemblage; however, the impetus to form microstructures such as biopyriboles might be chemical in nature. Metal/Si ratios of the non-stoichiometric 'intermediate microstructures' such as biopyribole will resemble Si-rich ferromagnesiosilica smectite-dehydroxylates [74].

Another type of non-stoichiometric mineral composition arises by incorporation of vacancy molecules in solid solution to maintain the integrity of the mineral structure, *e.g.* Mg-Eskola pyroxene $\square_{0.5}Mg_{0.5}Al[Si_2O_6]$ in pyroxenes. It is possible that metastable dehydroxylates in solid solution cause non-stoichiometry, *e.g.* "excess Si and Al" as a metastable kaolinite-dehydroxylate molecule. During thermal heat treatment this dehydroxylate decomposes as $Al_2Si_2O_7 \Rightarrow Al_2SiO_5 + SiO_2$ whereby the products will form inclusions in their host mineral. This scenario is consistent with the petrographic relationships of sillimanite needles observed in garnet. Sillimanite, instead of being a relict of an older metamorphic event, may have formed by decomposition of a metastable aluminosilica component. Admittedly, this scenario is entirely unproven but the point is that the "black box" could hide predictable metastable behavior during metamorphism.

## Layer silicates and the Origin of Life

Layer silicates, in particular clay minerals, defy our attempts to constrain thermodynamic equilibrium stability fields. It has been suggested that this group of minerals might not be 'true [equilibrium] phases' [80, among many others]. It is at least curious that the metal/Si ratios in most of the metastable eutectic dehydroxylates defined by the non-equilibrium gas-to-solid condensation experiments are identical to those of layer silicates (Table 5). This phenomenon indicates that their compositions may not be constrained by thermodynamic equilibrium but rather could reflect metastable behavior. This would provide such phases with considerable "internal chemical energy". Natural terrestrial greenalite is restricted to the unique Precambrian Banded Iron Formations wherein it precipitated from a gel [81] during a period in the geological past when iron oxidation favored greenalite formation. Greenalite occurs also in the matrix of type CM carbonaceous chondrite meteorites [35].

The deadly hand of equilibrium thermodynamics pressing on the origin of life is a major problem [82]: Life is a process that occurs far from equilibrium. One process that may be involved in the origin of life relies on the synergy between layer silicates and hydrocarbon and carbonaceous materials that also form layered structures [83,84, and references therein]. Mixed-layered stacks of carbonaceous materials and layer silicates are clearly not in equilibrium. Because both of these solids, each with predictable metastable eutectic compositions, occur in many natural environments, these mixed-layered stacks might become versatile components that could be quite responsive to environmental changes. This responsiveness to changing conditions is not limited to planetary environments. Carbons and layer silicates go hand-in-hand in even the most primitive materials such as IDPs [31,41,43] and thus probably also co-exist in comet nuclei. Mixed stacks of layer silicates with metastable eutectic metal/Si ratios and layered carbons could have played a vital catalytic role in the origin Life.

## SUMMARY

Chemical ordering at metastable eutectics was first recognized in non-equilibrium gas-to-solid condensation experiments conducted to constrain dust formation in O-rich circumstellar environments. Surprisingly, these types of metastable silicates might also have played a contributing role in the most exiting scientific enigma of all, the Origin of Life. Predictable metastable eutectic behavior follows directly from equilibrium thermodynamics. We were able to confirm this elusive feature experimentally. Now that we are able to recognize metastable eutectic behavior it opens the door to new and rewarding research opportunities that follow from the unique properties of these amorphous, typically nano- to micrometer-sized, materials. Many of the more exciting opportunities arise from the fact that such solids contain considerable "internal chemical and crystallographic free energy". Recognition has also demonstrated that metastable eutectic behavior is more common in many terrestrial and extraterrestrial environments than was preciously recognized.

**Acknowledgments** Drs. Robert Nelson and Susan Hallenbeck assisted with the condensation experiments in the Astrochemistry Branch at the NASA Goddard Space Flight Center. We are grateful to Prof. Janeczek who initiated the tropospheric fly ash program at the Faculty of Sciences, University of Silesia (Poland). MJ thanks Dr Sidsel Grundvig, Department of Earth Sciences (Århus University, Denmark) for access to the JEOL8600 SUPERPROBE. All AEM/TEM work was performed at the Electron Microbeam Analyses Facility in the Department

of Earth and Planetary sciences at UNM where Fleur Rietmeijer-Engelsman provided technical support. FJMR acknowledges financial support from NASA grant NAG5-4441.

## REFERENCES

[1] Prigogine, I. 1979, Astrophys. Space Sci., 65, 371.

[2] De, B.R. 1979, Astrophys. Space Sci., 65, 191.

[3] Nuth III, J.A. 1996, The Cosmic Dust Connection, J.M. Greenberg (Ed.), Kluwer Academic Publishers, 205.

[4] Nuth, III, J.A., Hallenbeck, S.L., and Rietmeijer, F.J.M. 1999, Laboratory Astrophysics and Space Research, P. Ehrenfreund, K. Krafft, H. Kochan, and V. Pirronello (Eds.), Kluwer Academic Publishers, Dordrecht, 143.

[5] Nuth III, J.A., Nelson, R.N., Moore, M., and Donn, B. 1988, Experiments on cosmic dust analogues, E. Bussoletti et al. (Eds.), Kluwer Academic Publishers, Dordrecht, 191.

[6] Nuth, J.A., and Donn, B. 1984, J. Geophys. Res., 89, Suppl., B657.

[7] Nelson, R., Nuth, J.A., and Donn, B. 1987, J. Geophys. Res., 92(B4), E657.

[8] Rietmeijer, F.J.M. 1995, Lunar Planet. Sci. XXVI, Lunar and Planetary Institute, Houston (TX), 1163.

[9] Rietmeijer, F.J.M., and Karner, J.M. 1999, J. Chem. Phys., 110(9), 4554.

[10] Rietmeijer, F.J.M., Nuth III, J.A., and Karner, J.M. 1999, Astrophys. J., 527, 395

[11] Rietmeijer, F.J.M., Nuth III, J.A., and Karner, J.M. 1999, Phys. Chem. Chem. Phys 1, 1511.

[12] Cliff, G., and Lorimer, G.W. 1975, J. Microscopy, 103, 203.

[13] Nuth, J.A., and Hecht, J.H. 1990, Astrophys. Space Sci., 163, 79.

[14] Aitken, D.K., and Roche, P.F. 1984, Galactic and Extragalactic Infrared Spectroscopy, M.F. Kessler, and J.P. Phillips (Eds.), Reidel Publishing Company, Dordrecht, 331.

[15] Tielens, A.G.G.M., and Allamandola, L.J. 1987, Interstellar Processes, D.J. Hollenbach, and H.A. Thronson (Eds.), Reidel Publishing Company, Dordrecht, 397.

[16] Sheffler, H., and Elsässer, H. 1987, Physics of the Galaxy and Interstellar Matter, Springer Verlag Berlin, Heidelberg, New York.

[17] Dorschner, J., Friedemann, C., Gürtler, J., and Henning, Th. 1988, Experiments on cosmic dust analogues, E. Bussoletti et al. (Eds.), Kluwer Academic Publishers, Dordrecht, 209.

[18] Leucci, F., Colangeli, L., Bussoletti, E., and Krätchmer, W. 1988, Experiments on cosmic dust analogues, E. Bussoletti et al. (Eds.), Kluwer Academic Publishers, Dordrecht, 231.

[19] Cheeseman, P., Stutz, J., Self, M., Taylor, W., Goebel, J., Volk, K., and Walker, H. 1989, NASA Reference Publ. 1217, GPO, Washington (DC), 592.

[20] Waters, L.B.F.M. et al. 1996, Astron. Astrophys., 315, L361.

[21] Waelkens, C. et al. 1996, Astron. Astrophys., 315, L245.

[22] Hallenbeck, S.L., Nuth, J.A., and Daukantas, P.L. 1998, Icarus, 131, 198.

[23] Rietmeijer, F.J.M. 1996, Meteoritics Planet. Sci., 31, 237.

[24] Rietmeijer, F.J.M., Nuth, J.A., and Mackinnon, I.D.R. 1986, Icarus, 65, 211.

[25] Nuth, J.A. 1987, Are small diamonds Astrophys. Space Sci., 139, 103.

[26] Rotundi, A., Rietmeijer, F.J.M., Brucato, J.R., Colangeli, L., Mennella, V., Palumbo, P., and Bussoletti, E. 2000, Planet. Space Sci., in press.

[27] Brownlee, D.E., Bates, B., and Schramm, L.S. 1997, Meteoritics Planet. Sci., 32, 157.

[28] Kurat, G., Koeberl, C., Presper, T., Brandstätter, F., and Maurette, M. 1994, Geochim. Cosmochim. Acta, 58, 3879.

[29] Kerridge, J.F., and Matthews, M.S. 1988, Meteorites and the Early Solar System, University Arizona Press, Tucson (AZ).

[30] Rietmeijer, F.J.M. 1998, Planetary Materials, Reviews Mineralogy, 36, J.J. Papike (Ed.), Mineralogical Society America, Washington, DC, 2-1.

[31] Rietmeijer, F.J.M. 1998, Advanced Mineralogy, Vol. 3, A.S. Marfunin (Ed.), Springer Verlag Berlin-Heidelberg, 22.

[32] Shearer, C.K., Papike, J.J., and Rietmeijer, F.J.M. 1998, Planetary Materials, Reviews Mineralogy, 36, J.J. Papike (Ed.), Mineralogical Society of America, Washington (DC), 1-1.

[33] Holweger, H. 1977, Earth Planet. Sci. Lett., 34, 152.

[34] Anders, E., and Ebihara, M. 1982, Geochim. Cosmochim. Acta, 46, 2363.

[35] Zolensky, M.E., and McSween Jr, H.Y. 1988, Meteorites and the Early Solar System, J.F. Kerridge, and M.S. Mathews (Eds.), University Arizona Press, Tucson (AZ), 114.

[36] Rietmeijer, F.J.M. 1999, Astrophys. J. 514, L125.

[37] Woolum, D.S., and Cassen, P.1999, Meteroritics Planet. Sci. 34, 897.

[38] Grossman, L., and Larimer, J.W. 1974, Reviews Geophys. Space Phys., 1, 71.

[39] Lewis, J.S. 1974, Science, 186, 440.

[40] Zolensky, M.E., Wilson, T.L., Rietmeijer, F.J.M., and Flynn, G.J. 1994, Analysis of Interplanetary Dust, Am. Inst. Phys. Conf. Proc., 310, Am. Inst. Physics Press, Woodbury (NY).

[41] Rietmeijer, F.J.M. 1992, Trends Mineralogy, 1, Council Scientific Research Integration, India, 23.

[42] Messenger, S., and Walker, R.M. 1997, Astrophysical implications of the laboratory study of presolar materials, T.J. Bernatowicz, and E.K. Zinner (Eds.), Am. Inst. Phys. Conf. Proc. 402, Am. Inst. Physics Press, Woodbury (NY), 545.

[43] Mackinnon, I.D.R., and Rietmeijer, F.J.M. 1987, Reviews Geophys., 25, 1527.

[44] Sandford, S.A. 1987, Fundamentals Cosmic Physics, 12, 1.

[45] Brownlee, D.E. 1985, Ann. Rev. Earth Planet. Sci., 13, 147.

[46] Grün, E., and Jessberger, E.K. 1990, Physics and Chemistry of Comets, W.F. Huebner (Ed.), Springer-Verlag Berlin, Heidelberg, New York, London, Paris, Tokyo, Hong Kong, Barcelona, 113.

[47] Brownlee, D.E., Joswiak, D.J., and Bradley, J.P. 1999, Lunar Planet Sci XXX, Lunar and Planetary Institute, Houston (TX), CD ROM #2031.

[48] Bradley, J.P. 1994, Science, 265, 925.

[49] Grieve, R.A.F. 1991, Meteoritics 26, 175.

[50] Hörz, F., Grieve, R., Heiken, G., Spudis, P., and Binder, A. 1991, Lunar Sourcebook, A user's guide to the Moon, G.H. Heiken, D.T. Vaniman, and B.M. French (Eds.), Cambridge University Press, Cambridge, New York, Port Chester, Melbourne, Sydney, 61.

[51] Stöffler, D., Bischoff, A., Buchwald, V., and Rubin, A.E. 1988, Meteorites and the Early Solar System, J.F. Kerridge, and M.S. Mathews (Eds.), University Arizona Press, Tucson (AZ), 165.

[52] Martinez, I., Schärer, U., and Guyot, F. 1993, Earth. Planet. Sci. Lett., 119, 207.

[53] Schaal, R.B. 1982, Contrib. Mineral. Petrol., 81, 39.

[54] Cosca, M.A., and Peacor, D.R. 1987, Am. Mineral., 72, 148.

[55] Cosca, M.A., Essene, E.J., Geissman, J.W., Simmons, W.B., and Coates, D.A. 1989, Am. Mineral., 74, 85.

[56] Foit, Jr., F.F., Hooper, R.L., and Rosenberg, P.E. 1987, Am. Mineral., 72, 137.

[57] Essene, E.J., and Fisher, D.C. 1986, Science, 234, 189.

[58] Rietmeijer, F.J.M., Karner, J.M., Nuth III, J.A., and Wasilewski, P.J. 1999, Eur. J. Mineral., 11, 181.

[59] Fischer, W.A., and Hoffmann, A. 1955, Arch. Eisenhüttenwerke, 26, 43.

[60] Gaudichet, A., Petit, J.R., Lefevre R., and Lorius C. 1986, Tellus, 38B, 250.

[61] Ram, M., and Gayley, R.I. 1991, Nature 349, 401.

[62] Zielinski, G.A., Dibb, J.E., Qinzhao, Yang, Mayewski, P.A., Whitlow, S., Twickler, M.S., and Germani, M.S. 1997, J. Geophys, Res., 102(D25), 30,031.

[63] Rietmeijer, F.J.M. 1993, J. Volc. Geothermal Res., 55, 69.

[64] Lefèvre, R., Gaudichet, A., and Billon-Galland, M.-A. 1985, Comptes Rendus Acad. Sci. Paris, Tome 301, Série II, 20, 1433.

[65] Lefèvre, R., Gaudichet, A., and Billon-Galland, M.-A. 1986, Nature 322, 817.

[66] Rietmeijer, F.J.M. 1988, J. Volc. Geothermal Res. 34, 173.

[67] Rietmeijer, F.J.M., and Janeczek, J. 1997, Atmospheric Environment 31, 1941.

[68] Jablonska, M. 1999, Ph.D. Thesis, The University of Silesia, Sosnowiec (Poland) (in Polish).

[69] Hulett, L.D., and Weinberger, A.J. 1980, Environ. Sci. Technol. 14, 965.

[70] Hulett, Jr., L.D., Weinberger, A.J., Northcutt, K.J., and Ferguson, M. 1980, Science, 210, 1356.

[71] Ondov, J.M., Zoller, W.H., Olmez, I., Aras, N.K., Gordon, G.E., Rancitelli, L.A., Abel, K.H., Filby, R.H., Shah, K.R., and Ragaini, R.C. 1975, Anal. Chem. 47, 1102.

[72] Zevenbergen, C., Bradley, J.P., van Reeuwijk, L.P., Shyam, A.K., Hjelmar, O., and Comans, R.N.J. 1999, Environ. Sci. Technol., 33, 3405.

[73] Watt, J.D., and Thorne, D.J. 1965, J. Appl. Chem., 15, 585.

[74] Rietmeijer, F.J.M. 1999, Am. Mineral., 84, 1883.

[75] Hochella, Jr., M.F. 1993, Health Effects of Mineral Dusts, G.D. Guthrie, Jr., and B.T. Mossman (eds.), Reviews Mineralogy, 28, Mineralogical Society of America, Washington (DC), 275.

[76] Paoletti, L., Falchi, M., Batisti, D., Carrieri, M.P., Petrelli, M.G., Ciallelli, C., and Donelli, G. 1991, Atmospheric Environment, 25B, 381.

[77] Bischoff, A., Rubin, A.E., Keil, K., and Stöffler, D. 1983, Earth Planet. Sci. Lett., 66, 1.

[78] Veblen, D.R. 1981, Amphiboles and other hydrous pyriboles-mineralogy, D.R. Veblen (Ed.), Reviews Mineralogy, 9A, Mineralogical Society of America, Washington (DC), 189.

[79] Akai, J. 1992, Contrib. Mineral. Petrol., 80, 117.

[80] May, H.M., Kinniburgh, D.G., Helmke, P.A., and Jackson, M.L. 1986, Geochimica Cosmochimica Acta, 50, 1667.

[81] Klein, C. 1983, Iron-formation: Facts and Problems, A.F. Trendall, and R.C. Morris (Eds.), Elsevier Science Publishers B.V., Amsterdam, 417.

[82] Maddox, J. 1994, Nature, 356, 409.

[83] Rietmeijer, F.J.M. 1991, Carbon, 29, 669.

[84] Rietmeijer, F.J.M. 1992, Geochim. Cosmochim. Acta, 56, 1665.

TABLE 1: Chemical compositions of condensed end-member and metastable eutectic solids in three binary systems. The notation 'FeO' is used without consideration of the actual $FeO/Fe_2O_3$ ratio (see text). A formula is given when the composition can be reduced to a structural formula with rational subscripts.

| Chemical System | $Al_2O_3$-$SiO_2$ | $FeO/Fe_2O_3$-$SiO_2$ | MgO-$SiO_2$ |
|---|---|---|---|
| End-members | Absent | 100-wt % $Fe_2O_3$ | 100-wt % MgO |
| | Absent | 97-wt % $Fe_2O_3$ | |
| Metastable eutectics | 47-wt % $Al_2O_3$; $Al_2Si_2O_7$ | | 50-wt % MgO; $Mg_3Si_2O_7$ |
| | | 33-wt % 'FeO', $^{2+}Fe_5Fe^{3+}[Fe^{3+}Si_7]O_{22}$ | 28-wt % MgO; $Mg_6Si_8O_{22}$ |
| | 11.5-wt % $Al_2O_3$ | 17-wt % 'FeO' | |
| End-member | 100-wt % $SiO_2$ | 100-wt % $SiO_2$ | 100-wt % $SiO_2$ |

TABLE 2: Silicate minerals constrained in the MgO-'FeO'-$SiO_2$ system

| OLIVINE | PYROXENE | LAYER SILICATES |
|---|---|---|
| $(Mg,Fe)_2SiO_4$ | $(Mg,Fe)_2Si_2O_6$ | Serpentine – Greenalite, $(Mg,Fe)_3Si_2O_5(OH)_4$ |
| | | Talc – Minnesotaite, $(Mg,Fe)_6Si_8O_{20}(OH)_4$ |
| | | Saponite - Fe-saponite, |
| | | $\{Mg_6Si_8 - {}^{2+}Fe_5Fe^{3+}[Fe^{3+}Si_7]\}O_{20}(OH)_4 \cdot X^{+} \cdot nH_2O$ |

TABLE 3: Mean ± one standard deviation and range of $Al_2O_3$ (wt %) content of metastable eutectic and heat-treated solids in the $Al_2O_3$-$SiO_2$ phase diagram [9], and the compositions of tropospheric and stratospheric volcanic dust [60-65], airborne fossil-volcanic fly ash in USIR (ATEM data; [67,68] and SEM/EMPA data; [68]. The Student's t-test for populations means (5% significance level) shows no evidence that the samples listed in each column are from populations with a different mean than the means of the metastable eutectics

| | | | | | |
|---|---|---|---|---|---|
| Metastable eutectics [9] | 6.7 ± 3.0 | 11.5 ± 3.0 | | 46.7 ± 10.8 | |
| Range | 1 – 15 | 6 – 16 | | 21.8 – 71.3 | |
| Annealed solids [9] | 9.2 ± 3.1 | | 26.6 ± 4.4 | 41.4 ± 5.4 | 59.7 ± 5.6 |
| Range | 3.3 – 15.4 | | 20.8 – 37.1 | 32.0 – 55.1 | 50.0 – 68.9 |
| Volcanic dust [60-65] | 3.8 ± 0.4 | 12.4 ± 2.7 | 23.4 ± 5.2 | | |
| Range | 3.5 –4.3 | 9.0 – 15.5 | 16.1 – 34.7 | | |
| Fossil volcanic dust [67,68] | 5.9 ± 1.3 | 11.5 ± 2.4 | 22.6 ± 4.3 | | |
| Range | 3.0 – 7.7 | 8.0 – 16.0 | 16.7 – 37.0 | | |
| Fossil volcanic dust [68] | | | 22.2 ± 1.8 | 40.1 ± 5.0 | |
| Range | | | 18.8 – 26.4 | 37.1 – 53.3 | |

TABLE 4: Mean ± one standard deviation and range of $Al_2O_3$ (wt %) contents in metastable eutectic and heat-treated solids in the $Al_2O_3$-$SiO_2$ phase diagram [9] and the compositions of aluminosilica coal fly ash spheres <10-wt% 'others'. The Student's t-test for population means (5% significance level) shows no evidence that the metastable eutectic kaolinite dehydroxylate solids [9] and coal fly ash spheres [69-73] and [68] are from populations with different means.

| | | | | | |
|---|---|---|---|---|---|
| Metastable eutectics [9] | 6.7 ± 3.0 | 11.5 ± 3.0 | | 46.7 ± 10.8 | |
| Range | 1 – 15 | 6 – 16 | | 21.8 – 71.3 | |
| Annealed solids [9] | 9.2 ± 3.1 | | 26.6 ± 4.4 | 41.4 ± 5.4 | 59.7 ± 5.6 |
| Range | 3.3 – 15.4 | | 20.8 – 37.1 | 32.0 – 55.1 | 50.0 – 68.9 |
| Fly ash spheres [69-73] | | | | 39.2 ± 1.6 | |
| Range | | | | 36.5 – 40.9 | |
| Fly ash spheres [68] | 8.2 ±0.7 | | 25.6 ± 4.0 | 38.8 ± 3.3 | |
| Range | 2.1 – 12.6 | | 14.8 – 34.5 | 32.1 – 54.7 | |

TABLE 5: Metastable eutectic dehydroxylate compositions due to non-equilibrium gas-to-solid condensation and heat-treatment (*) in the systems $Al_2O_3$-$SiO_2$, $FeO/Fe_2O_3$-$SiO_2$ and MgO-$SiO_2$ with the structural formulae of the matching layer silicate minerals.

| | | | |
|---|---|---|---|
| $Al_2Si_2O_7$ | Kaolinite, $Al_2Si_2O_5(OH)_4$ | $Al_4Si_8O_{22}$ (*) | Pyrophyllite, $Al_4Si_8O_{20}(OH)_4$, and $Al_4Si_8O_{20}(OH)_4.X^+.nH_2O$, Illite |
| $Fe_3Si_2O_7$ | Greenalite, $Fe_3Si_2O_5(OH)_4$ | $^{2+}Fe_5Fe^{3+}[Fe^{3+}Si_7]O_{22}$ | $^{2+}Fe_5Fe^{3+}[Fe^{3+}Si_7]O_{20}(OH)_4.X^+.nH_2O$, Fe-saponite |
| $Mg_3Si_2O_7$ | Serpentine, $Mg_3Si_2O_5(OH)_4$ | $Mg_6Si_8O_{22}$ | $Mg_6Si_8O_{20}(OH)_4.X^+.nH_2O$, saponite, and $Mg_6Si_8O_{20}(OH)_4$, Talc |

**Fig. 1** Transmission electron micrograph showing aluminosilica grains that were condensed from an Al–SiO-$H_2$-$O_2$ vapor [9]. This fluffy (porous) texture is typical for the materials produced in the non-equilibrium gas-to-solid condensation experiments. Condensed pure silica grains occur as large dispersed aggregates within this fluffy material. Note variations in the condensed grain size that may show a weak correlation with the chemical composition. The gray background is the embedding epoxy used to prepare the ultramicotomed thin-section.

**Fig. 2** Transmission electron micrograph of an autoannealed, compact polycrystalline tridymite aggregate with an irregular circumference formed via condensation in an Fe–SiO-$H_2$-$O_2$ vapor. The typical tridymite twinning is visible in the upper portion of this compact grain. The gray background is the embedding epoxy of the ultrathin section (modified after ref. [11]).

**Fig. 3** Transmission electron micrograph of two amorphous pure silica spheres in ferrosilica materials that was condensed from an Fe–SiO-$H_2$-$O_2$ vapor and subsequently heat-treated in vacuo at 1000K for 4 hours. The spheres resulted from a solid-state amorphization transformation of compact polycrystalline tridymite aggregates (see Fig. 2).

**Fig. 4** The $Al_2O_3$-$SiO_2$ phase diagram showing the metastable aluminosilica eutectics at 11.5 and 47-wt % $Al_2O_3$ at the nominal quench temperature of 775K (black squares) and one of two aluminosilica solid compositions on the spinodal solvus limb after heat-treatment of the kaolinite metastable eutectic solids (open square). The metastable eutectic at 7-wt % $Al_2O_3$ of condensed, rimmed aluminosilica grains is not shown. Modified after ref. [9] with the original references to the phase diagrams.

**Fig. 5** The (pseudo) binary system FeO/$Fe_2O_3$-$SiO_2$ with the metastable eutectic compositions of condensed solids (open squares) at 97-wt % 'FeO' (in both diagrams), at 17-wt % 'FeO' (FeO/$Fe_2O_3$ = 8/2) and 33-wt % 'FeO' (FeO/$Fe_2O_3$ = 6/4) at the nominal quench temperature of 775K. The predicted composition of the $Fe_3Si_2O_7$, *i.e.* or metastable greenalite-dehydroxylate eutectic is also shown. Modified after ref. [11].

**Fig. 6** The MgO-$SiO_2$ phase diagram with the condensed solid compositions of the serpentine-dehydroxylate, $Mg_3Si_2O_7$, and smectite-dehydroxylate, $Mg_6Si_8O_{22}$, metastable eutectic points at the nominal quench-temperature of 775K. The data support a high-MgO-silica metastable

eutectic, which would require a modification of the original diagram (question mark) according to the long-dashed lines. Modified after refs. [4,10].

**Fig. 7** The ternary diagram MgO-FeO-$SiO_2$ (wt % oxides) with the chemical compositions of gas to solid condensed solids from a Fe-Mg-SiO-$H_2$-$O_2$ vapor with metastable "MgSiO' and 'FeSiO' solids (diamonds) matching the metastable eutectics in the individual binary systems (Figs. 5,6). The gas phase composition (dot) is taken to be similar to the "average bulk solid" composition obtained by AEM analyses although it was probably somewhat less 'SiO'-rich. The open arrow indicates the condensed solid compositions of the greenalite-dehydroxylate eutectic (see Fig. 5). Modified after ref. [10].

**Fig. 8** Scanning electron micrograph of the aggregate interplanetary dust particle W7017B2 with an approximately chondritic bulk composition (within a factor of 2). The scale bar is two micrometers. This particle is from the NASA Johnson Space Center Cosmic Dust Collection. This figure was modified after Rietmeijer and Warren in ref. [40]. Reproduced by courtesy of the National Aeronautics and Space Administration.

**Fig. 9** The Mg-Fe-Si (element wt %) diagram showing the mixing lines (dashed) between the condensed amorphous metastable eutectic solids (dots): (1) smectite (Sm-d) and serpentine (S-d) dehydroxylates, (2) the low-FeO ferrosilica dehydoxylates, (3) the Si-rich Fe- and Mg-oxides, and (4) common silica grains (solid square). The compositions of three coarse-grained smectite dehydroxylate, $(Mg,Fe)_6Si_8O_{22}$, units in an aggregate IDP matrix (black diamonds) represent the maximum element ratio Fe/(Fe+Mg) (*fe*) = 0.36 (line 1) and average ratio of 0.23 (line 2). A metastable serpentine dehydroxylate mixing line (dashed) connecting the S-d and greenalite (G-d) (open circle) metastable eutectics (see Fig 7) is located in between the stoichiometric olivine (Fo-Fa) and pyroxene (En-Fs) lines. The bulk compositions of all ultrafine-grained serpentine dehydroxylate, $(Mg,Fe)_3Si_2O_7$, units(*fe* = 0.36 – 0.83) plot on this particular mixing line [30]. The apex notation $Fe^{2+}$,$Fe^{3+}$ symbolizes variable $Fe^{2+}$/ $Fe^{3+}$ ratios. Modified after ref. [10].

**Fig. 10** The same Mg-Fe-Si (element wt %) diagram as Figure 9 showing the olivine composition (open square labeled O), the starting mixture of this olivine plus silica (open square labeled S) and melt compositions obtained at shock peak-pressures between 42.9 GPa and 64.2 GPa of this mixture (open squares). The data are from reference [53]. The melt compositions cluster tightly at the intersection of two mixing lines between metastable eutectic ferrosilica and

magnesiosilica solid composition. The compositions of the starting materials and the melts are close to line 2 of constant Fe/(Fe+Mg) (element ratio)

**Fig. 11** Transmission electron micrographs of coal fly ash due to inefficient coal burning in the Upper Silesian Industrial Region (Poland) collected at 95m above ground level [67]. On the left is shown a hollow silica sphere and on the right are two massive irregular aluminosilica shards. The grains are attached to fibers (arrowheads) of the dust collection substrate. The gray background is the holey carbon thin-film that is supported on a standard Cu-mesh grid for TEM analyses onto which the collected grains plus collection substrate were dispersed (see ref. [67] for details).

**Fig. 12** Transmission electron micrograph of a spongy (frothy or porous) aluminosilica shard among coal fly in the Upper Silesian Industrial Region (Poland) collected at 60m above ground level [68] attached to fibers (arrowheads) of the collection substrate (see caption fig. 11).

**Fig. 13** Scanning electron micrograph showing a porous alumniosilica coal fly conglomerate of spheres and irregularly-shaped particles collected at 90 meters above ground level in the city of Katowice in the Upper Silesian Industrial Region (Poland) [68].

1 µm

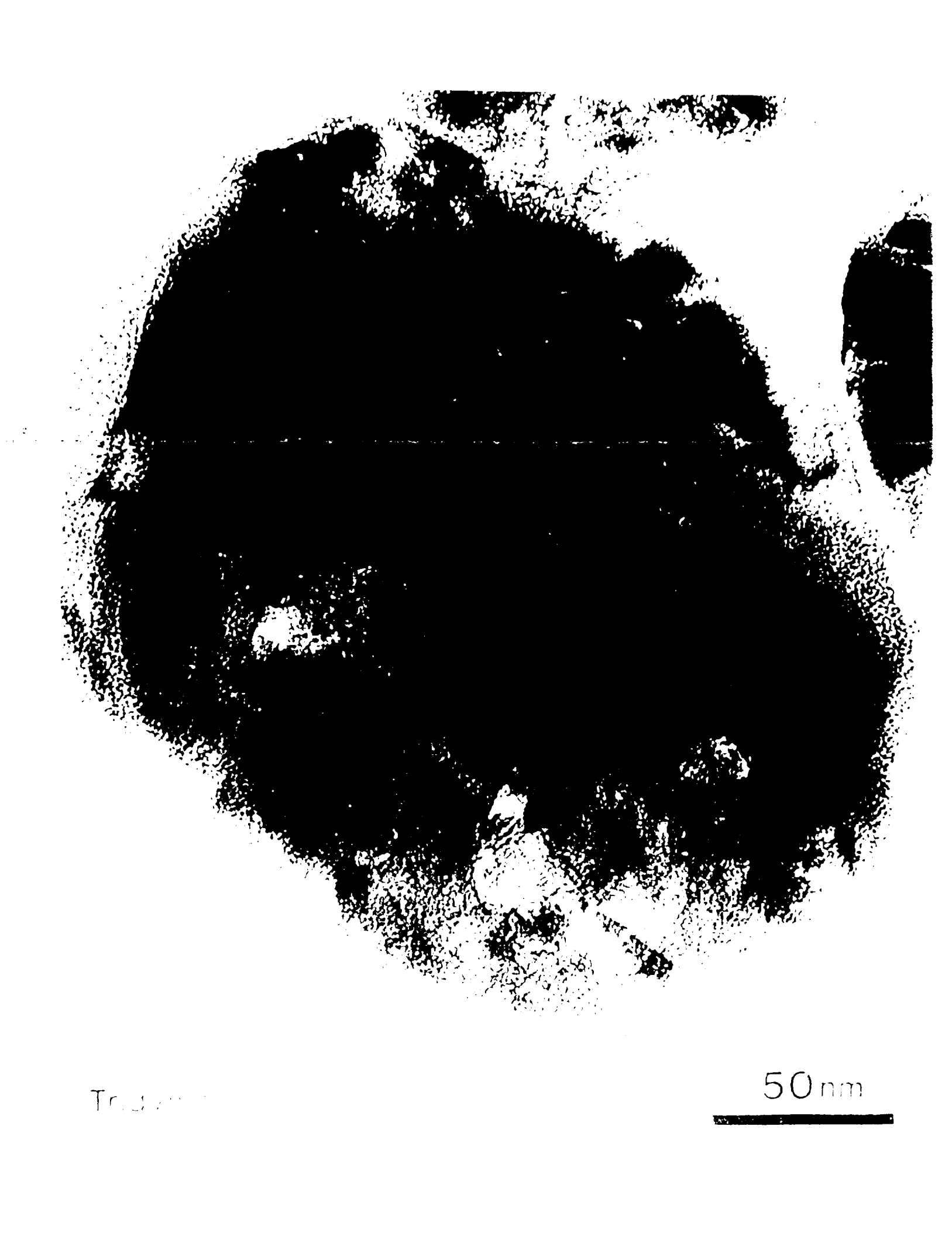
50nm

nm

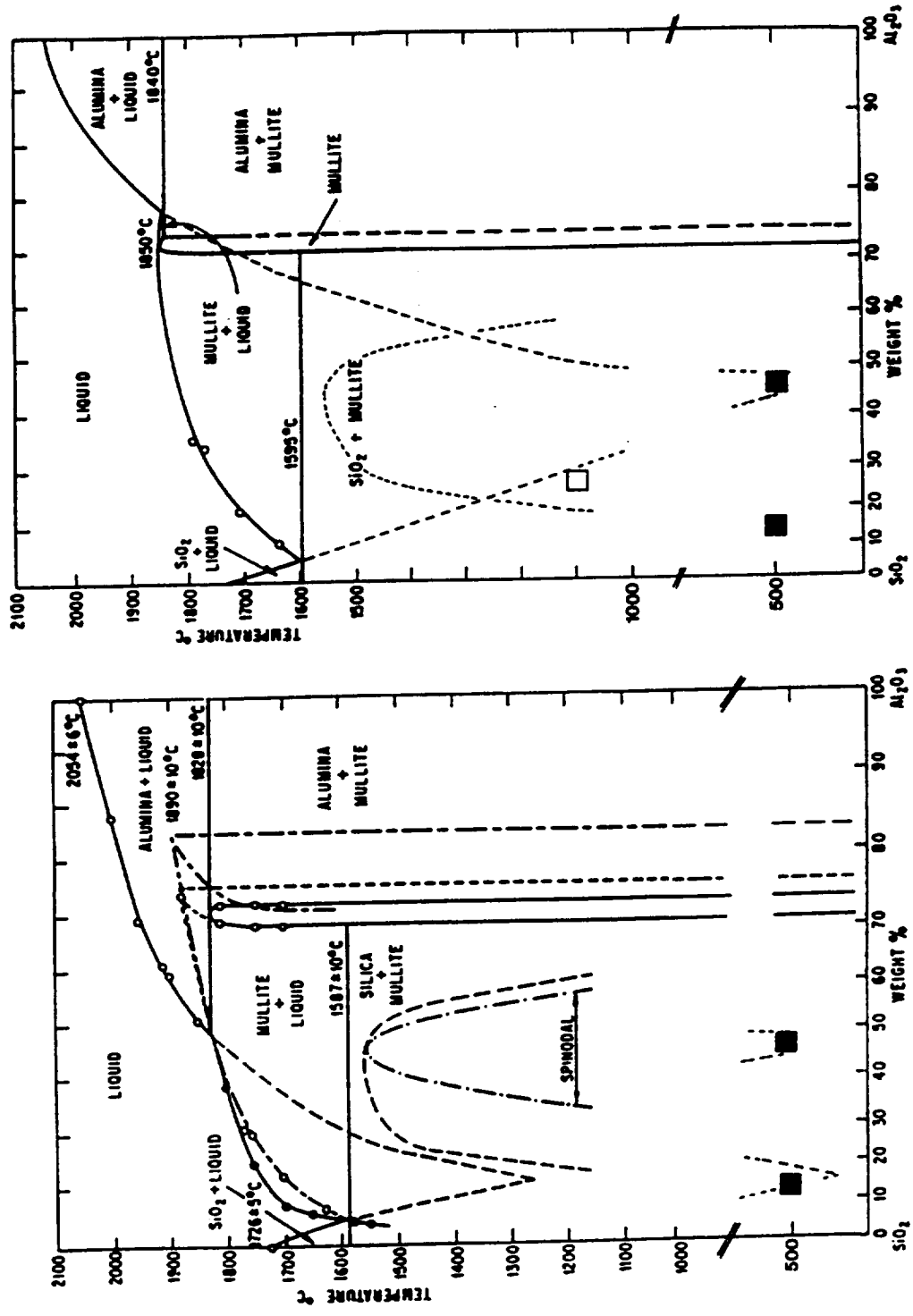
LIQUID
ALUMINA + LIQUID
1840°C
1850°C
ALUMINA + MULLITE
MULLITE
MULLITE + LIQUID
1595°C
SiO2 + MULLITE
SiO2 + LIQUID
TEMPERATURE °C
WEIGHT %
SiO2
Al2O3
LIQUID
ALUMINA + LIQUID
2054±6°C
1890±10°C
1828±10°C
ALUMINA + MULLITE
MULLITE + LIQUID
1587±10°C
SILICA + MULLITE
SPINODAL
SiO2 + LIQUID
1726±5°C

Fig 4

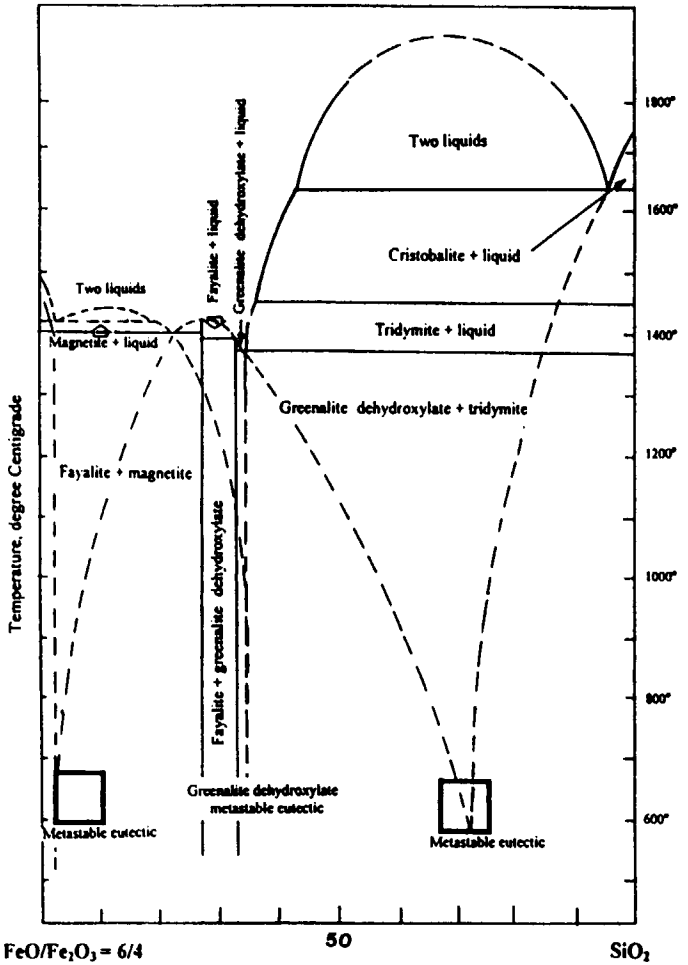
Two liquids
Cristobalite + liquid
Tridymite + liquid
Two liquids
Magnetite + liquid
Fayalite + liquid
Greenalite dehydroxylate + liquid
Greenalite dehydroxylate + tridymite
Fayalite + magnetite
Fayalite + greenalite dehydroxylate
Greenalite dehydroxylate metastable eutectic
Metastable eutectic
Metastable eutectic
Temperature, degree Centigrade
1800°
1600°
1400°
1200°
1000°
800°
600°
FeO/Fe2O3 = 6/4
50
SiO2

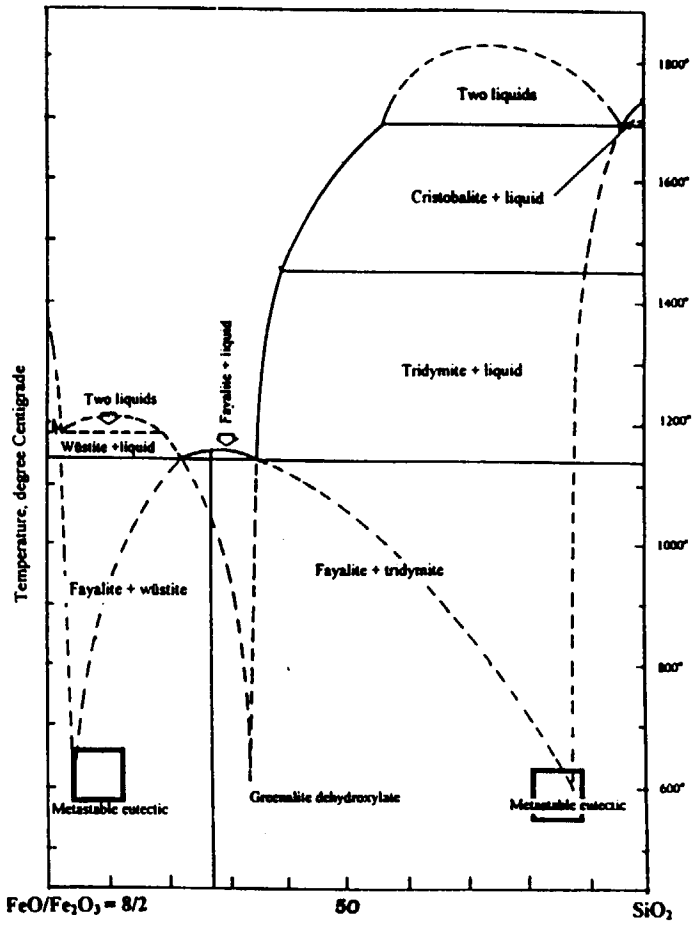
Two liquids
Cristobalite + liquid
Tridymite + liquid
Two liquids
Wüstite +liquid
Fayalite + liquid
Fayalite + wüstite
Fayalite + tridymite
Metastable eutectic
Greenalite dehydroxylate
Metastable eutectic
Temperature, degree Centigrade
1800°
1600°
1400°
1200°
1000°
800°
600°
FeO/Fe2O3 = 8/2
50
SiO2

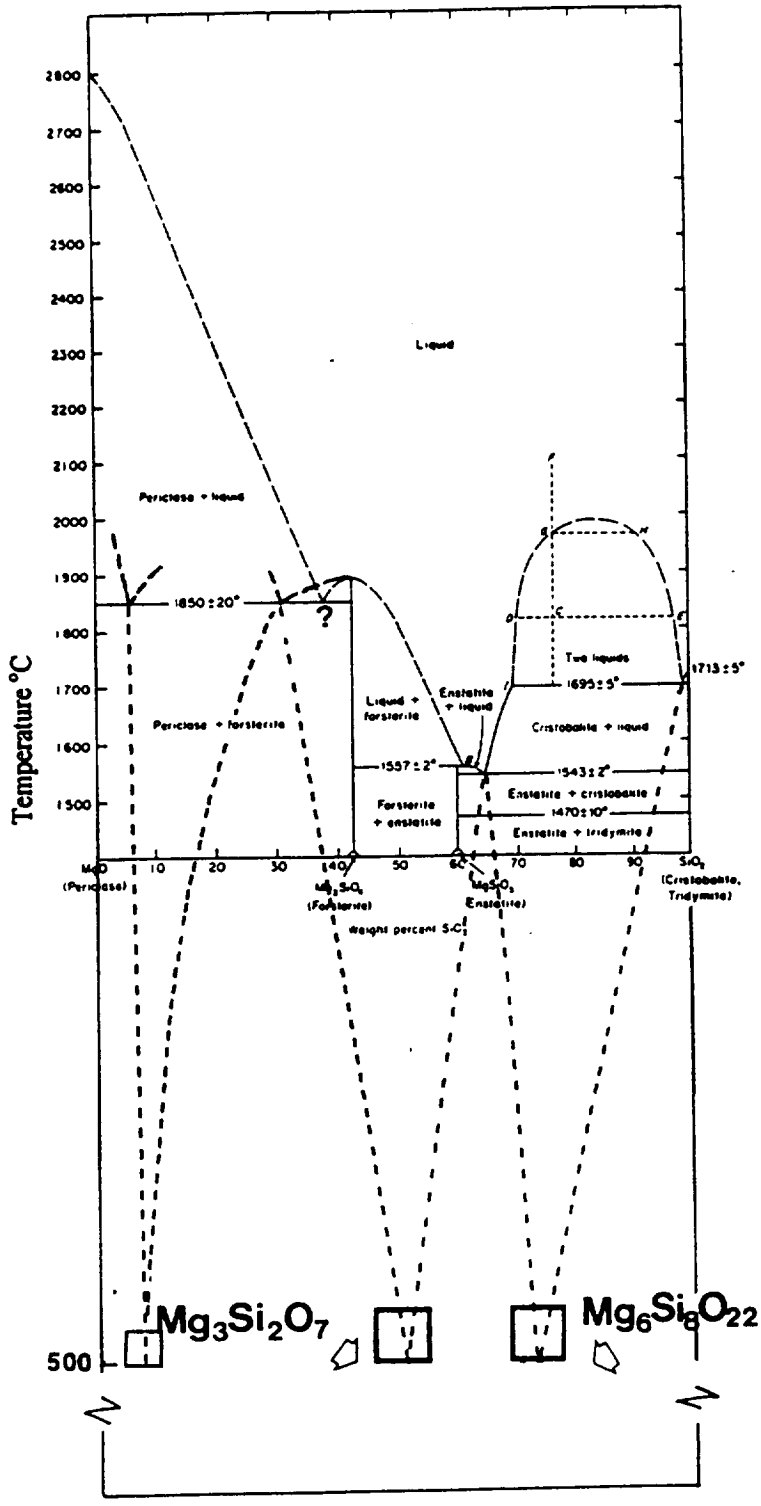
Temperature °C
2800
2700
2600
2500
2400
2300
2200
2100
2000
1900
1800
1700
1600
1500
500
Liquid
Periclase + liquid
1850 ± 20°
?
Periclase + forsterite
Liquid + forsterite
Forsterite + enstatite
1557 ± 2°
Enstatite + liquid
Two liquids
1695 ± 5°
1713 ± 5°
Cristobalite + liquid
1543 ± 2°
Enstatite + cristobalite
1470 ± 10°
Enstatite + tridymite
MgO (Periclase)
10
20
30
40
50
60
70
80
90
SiO2 (Cristobalite, Tridymite)
Mg2SiO4 (Forsterite)
MgSiO3 Enstatite)
weight percent SiO2
Mg3Si2O7
Mg6Si8O22

Pl56

Fig. 7

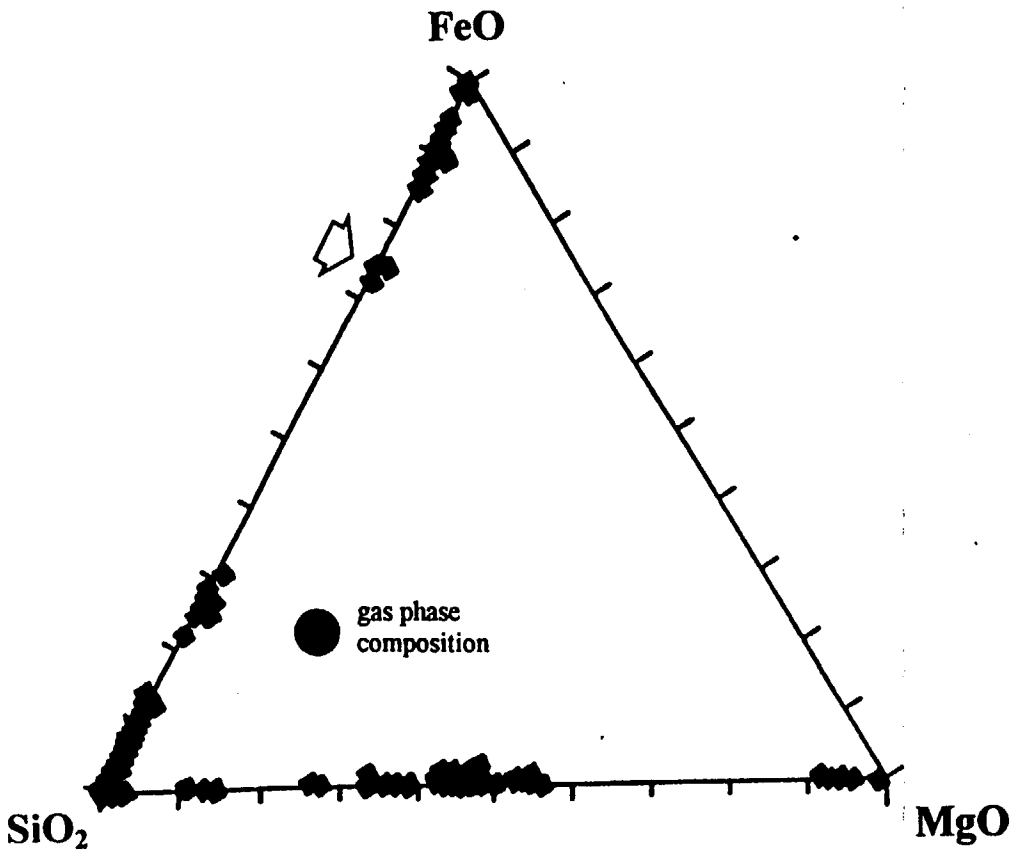

Fig 8

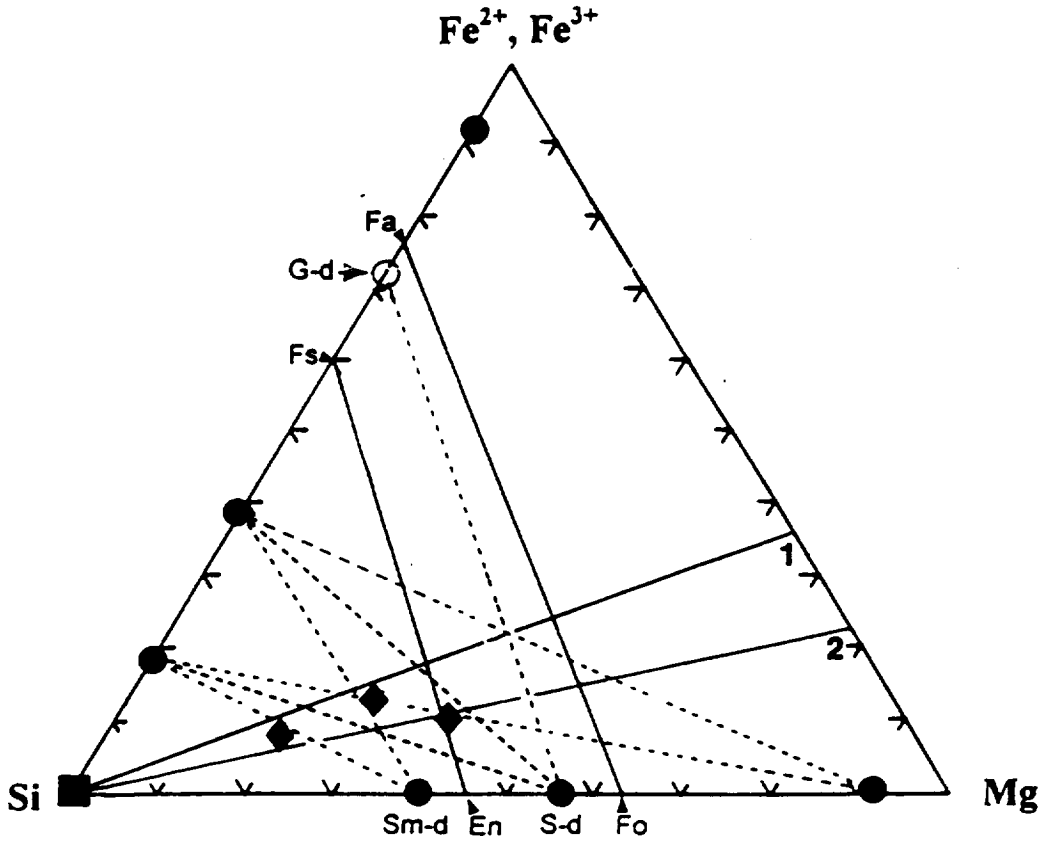


Fig 9

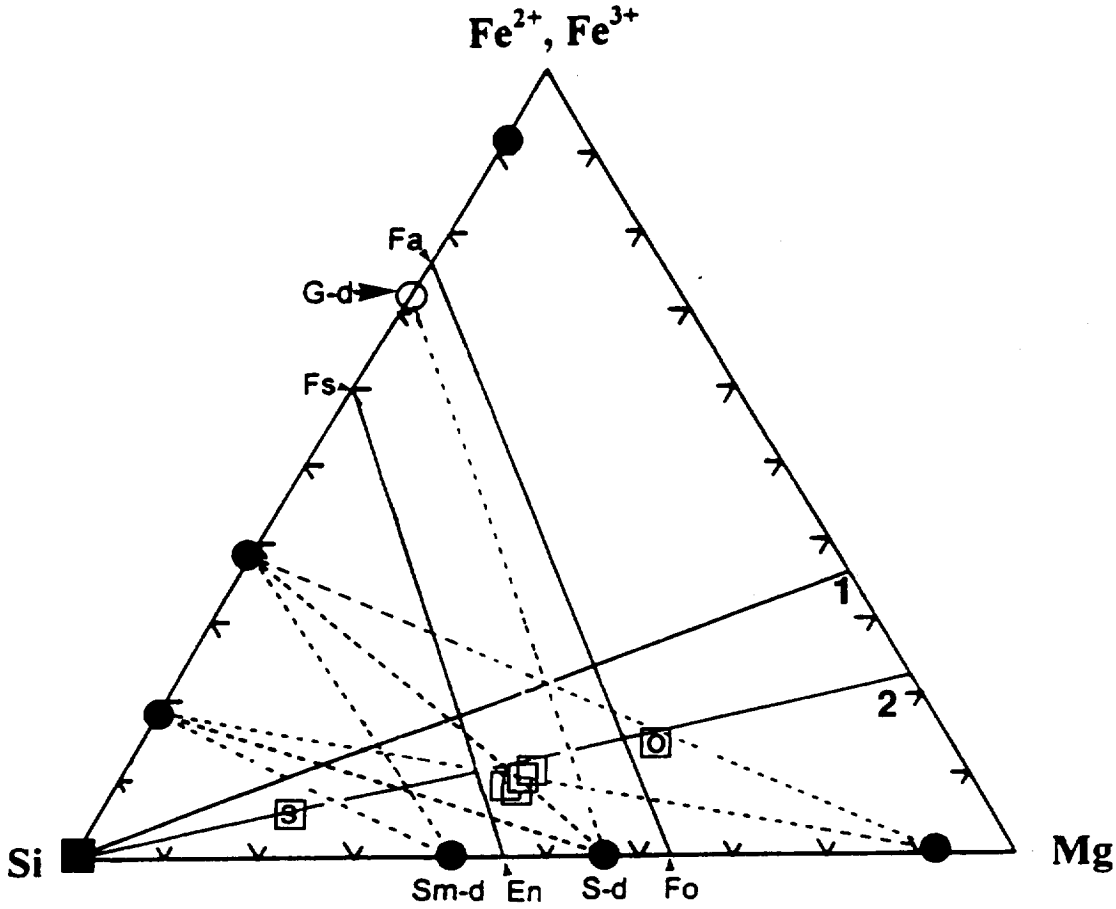


Fig 10

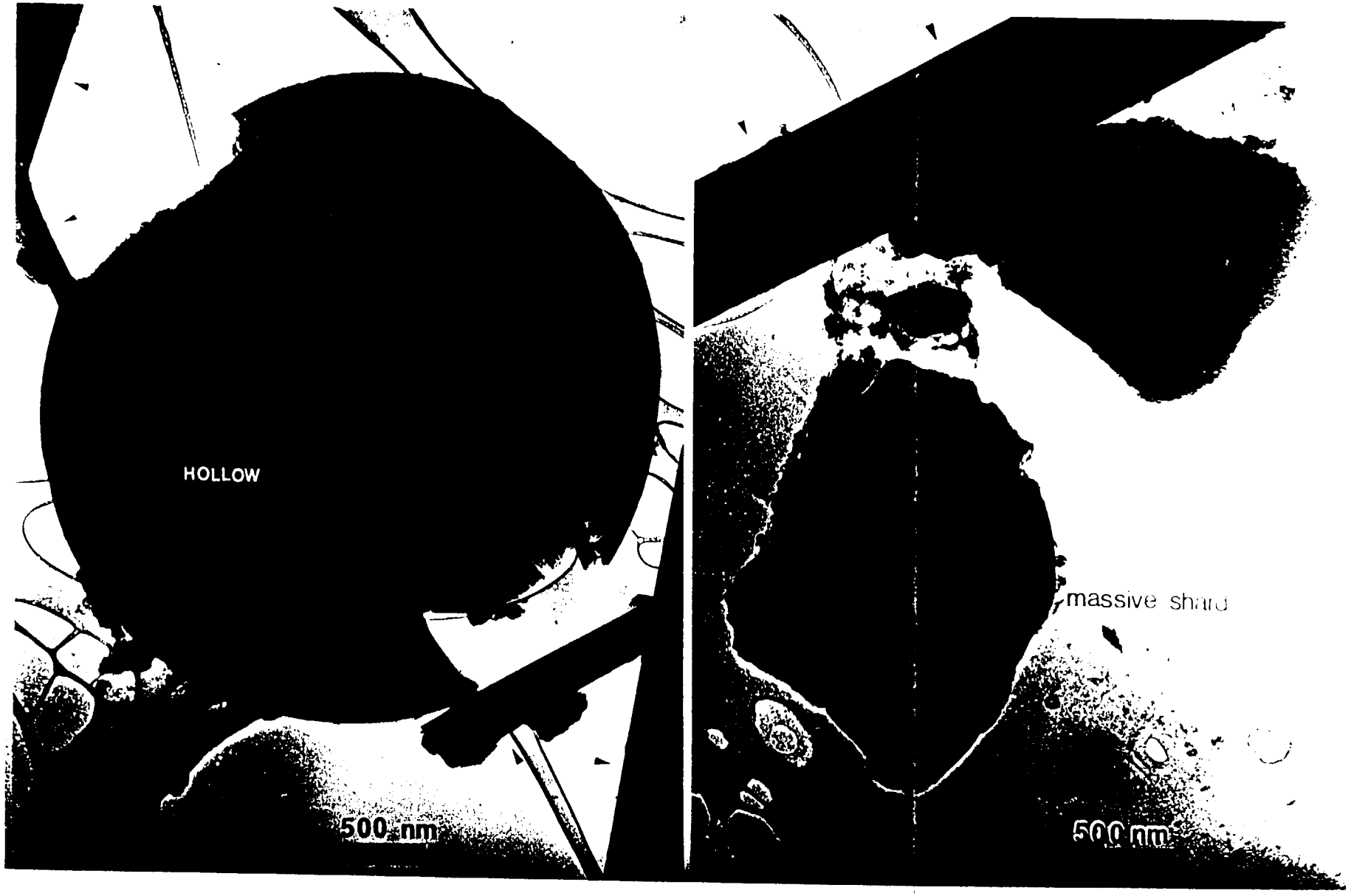
HOLLOW
500 nm
massive shard
500 nm

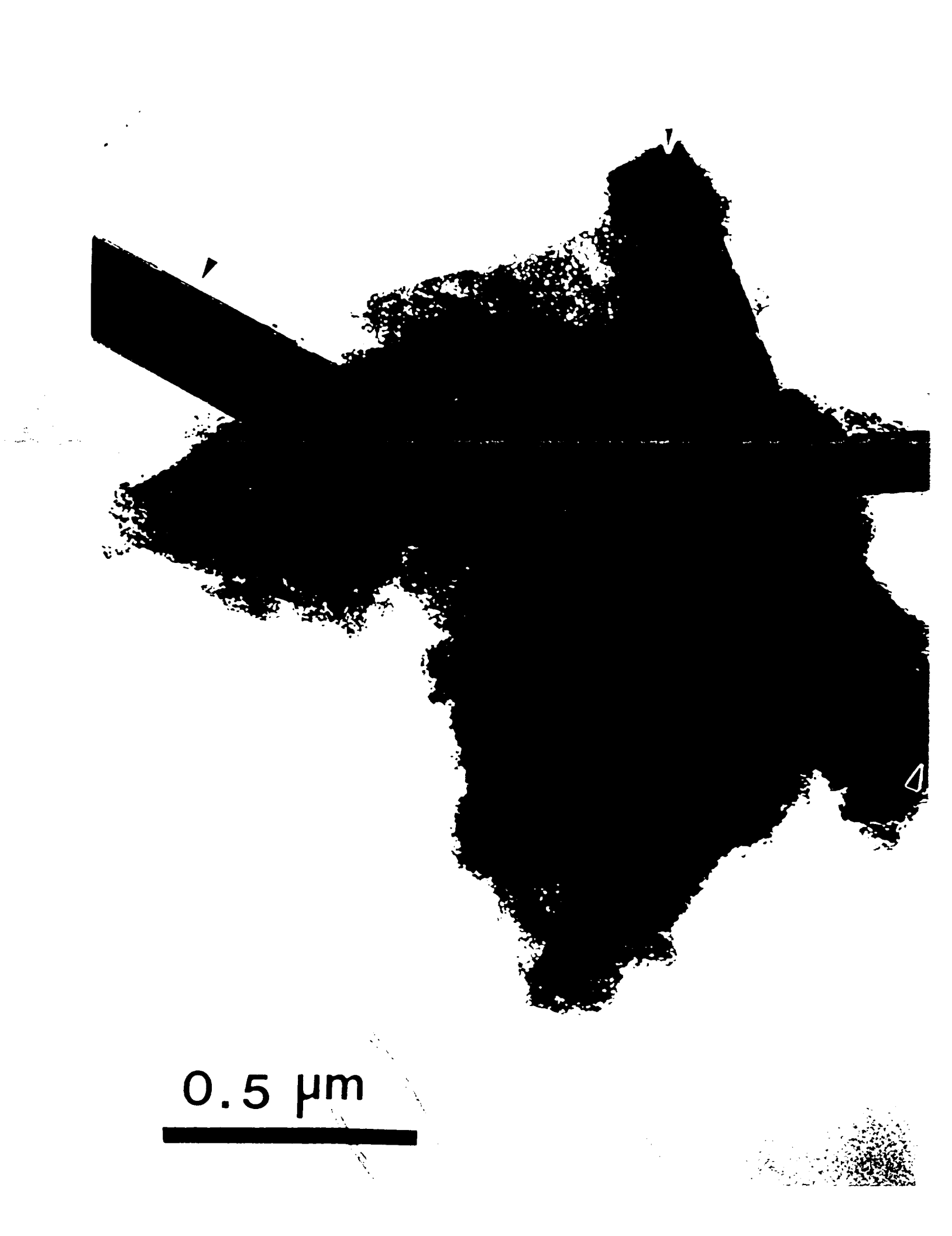
0.5 μm


Fig